ESA–MOST China Dragon 4 Cooperation

→ ADVANCED TRAINING COURSE IN OCEAN AND COASTAL REMOTE SENSING

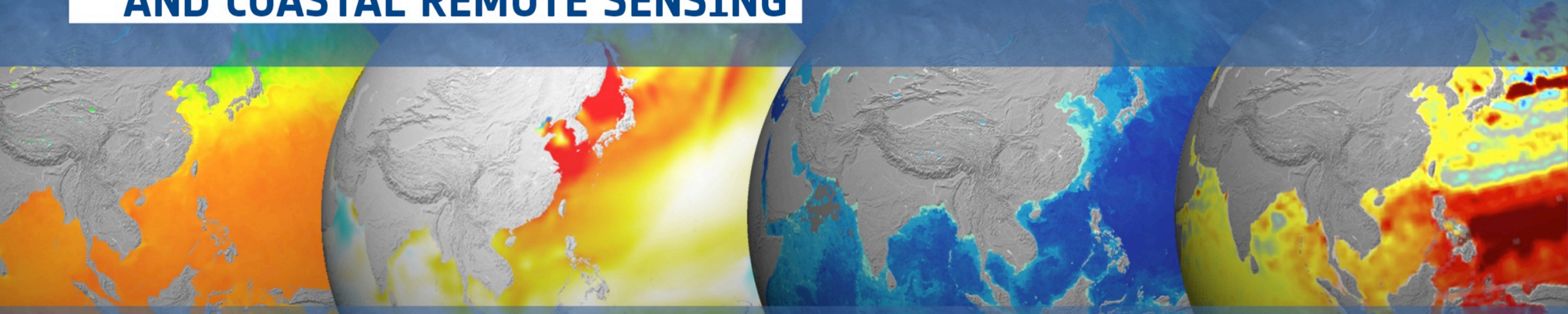

12 to 17 November 2018 | Shenzhen University | P.R. China

“Measurement of atmospheric phenomena over the ocean by SAR”, Werner Alpers

Hosted by

Introduction

- **Synthetic aperture radars (SARs) use microwaves.**
- **Microwaves penetrate clouds, but do not penetrate into the water body.**
- **SAR can detect oceanic and atmospheric phenomena over the ocean only via variations of the sea surface roughness.**

Oceanic phenomena can also be seen optical images via changes of the sea surface roughness, in particular in the sunglint area

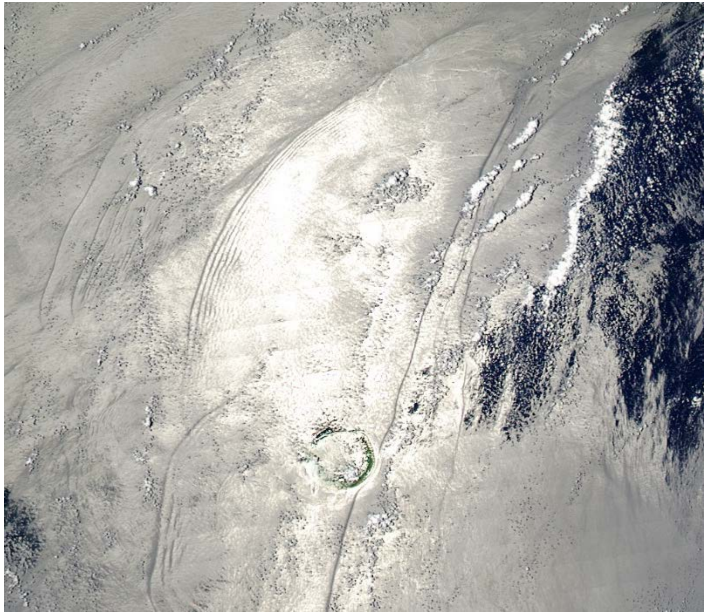

Here: Image taken in the sunglint area in the South China Sea

MODIS Aqua image,

03-11-2005,14:15UTC

Atmospheric phenomena in the marine boundary layer become visible on radar images acquired over the ocean because

- they are associated with a variable wind speed (or wind stress) at the sea surface, which
- modifies the sea surface roughness and thus
- modifies the backscattered radar power or Normalized Radar Cross Section (NRCS or σ_0).

Radar scattering at the sea surface at oblique incidence angles can be described by **Bragg scattering theory**

Ocean wave

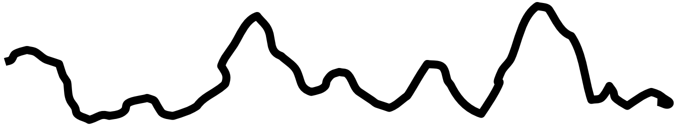

Fourier components of the ocean wave

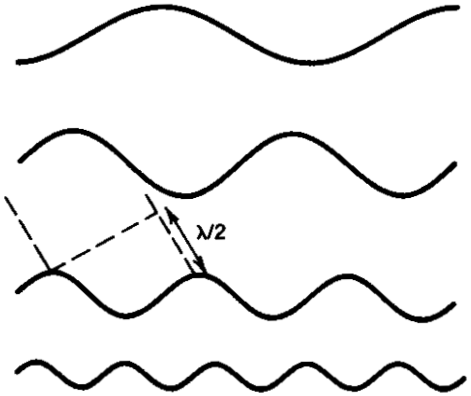

Bragg wave

William Henry Bragg, 1862-1942, Nobel prize 1915 for the analysis of the structure of crystals

The ocean wave field is decomposed into Fourier components, i.e., in a sum of ocean waves of different wavelength. Radar backscattering occurs only at those ocean waves, called “Bragg wave“, which obey the “Bragg resonance condition“.

Only those ocean surface waves contribute to the radar backscattering that obey the „Bragg resonance condition“:

$$\frac{\lambda_0}{2\sin\theta} = \lambda_B$$

λ_B = wavelength of the surface wave = „Bragg wave“

λ_0 = radar wavelength

θ = incidence angle

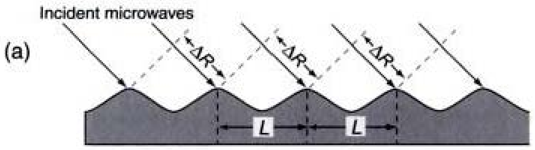

Synthetic aperture radar (SAR) is an ultra-sensitive instrument for measuring changes in the small-scale sea surface roughness.

Small - scale: 2- 30 cm

Small-scale changes in the sea surface roughness can be caused by

1. oceanic phenomena

2. atmospheric phenomena.

Dependence of the NRCS on Wind Speed

Experiments have revealed that the dependence σ^0 on wind speed **U** can be described by

$$\sigma^0 = a\mathbf{U}^b$$

a,b = empirically-derived coefficients

b $\approx$ 1 for L-band (Seasat SAR)

$\approx$ 1.5 for C-band SAR (ERS SAR, Radarsat,Envisat SAR)

$\approx$ 2 for X-band SAR (TerraSAR)

Atmospheric Phenomena detectable on SAR images acquired over the ocean:

Wind fronts
Atmospheric gravity waves
Atmospheric boundary layer rolls
Atmospheric eddies
Land-sea breeze
Katabatic winds
Rain ells
Atmospheric convective cells
Gap wind
Barrier jets
Island wakes

Wind fronts

Wind front over the South China Sea near Hong Kong (HK) generated by a sudden increase of the monsoon wind

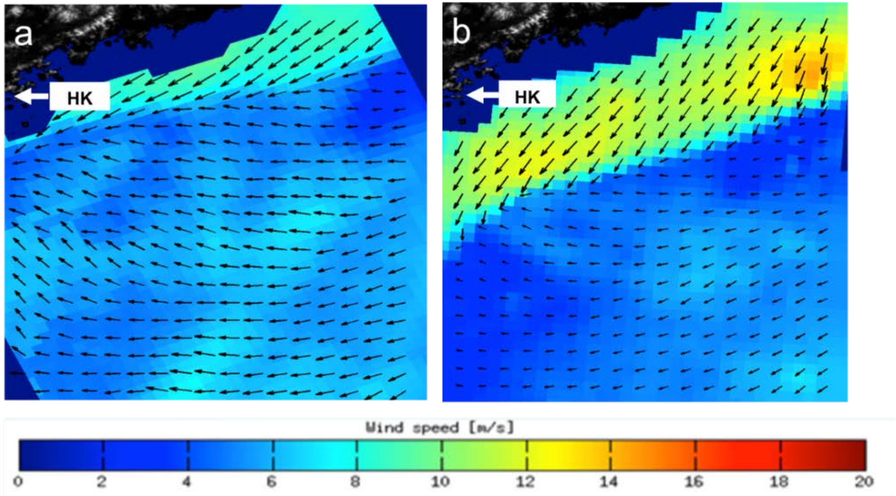

Scatterometer winds
Resolution: 25 km

Near-surface wind field retrieved from data of the ASCAT scatterometer onboard the MetOp satellite on (a) 29-12-2009 at 1358 UTC (2158 HKT) and (b) 30-12-2009 at 0227 UTC (1029 HKT).

From Alpers et al., Boundary Layer Meteorology, 2015

Details of wind front on Envisat SAR image

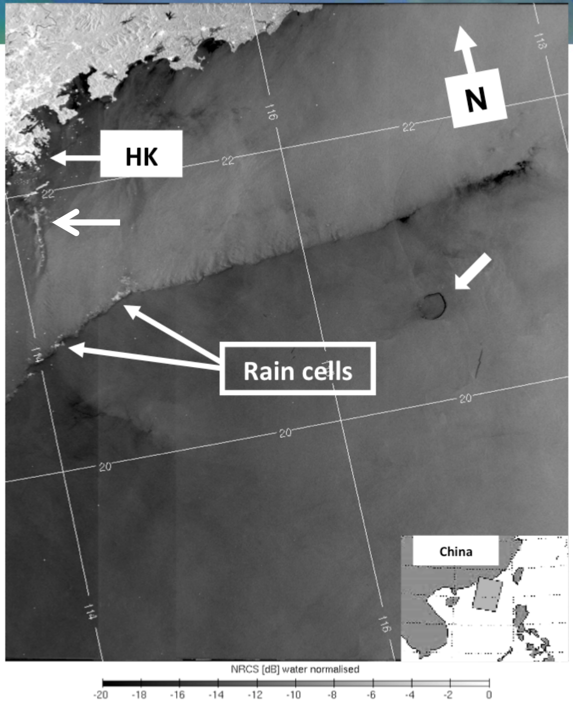

ENVISAT SAR image, 30-12-2009, 0213 UTC (1013 HKT), Chinese coast of the South China Sea near Hong Kong (HK). The black circle-like feature marked by a broad white arrow is the coral reef of Dongsha island. The imaged area is 510 km x 660 km. The inset shows the location of the SAR scene in the South China Sea.

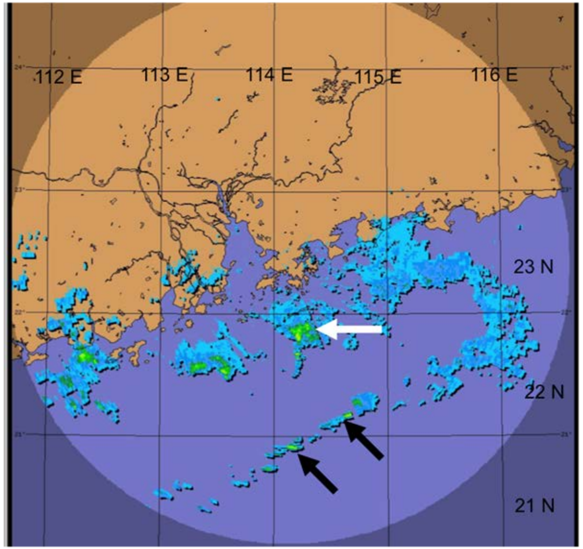

Weather radar image from the Hong Kong Observatory, 30-12-2009, 0212 UTC showing rain cells embedded in the front.,

Zoom on rain cells

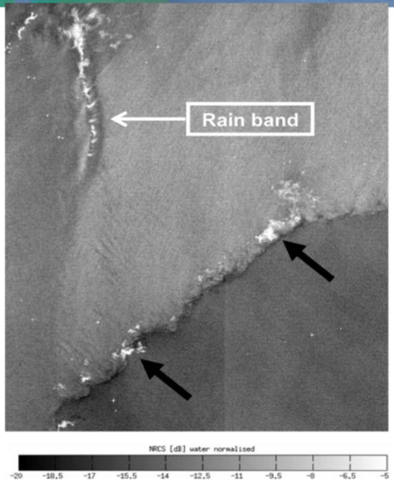

ENVISAT SAR image, 30-12-2009, 0213 UTC .

Model wind

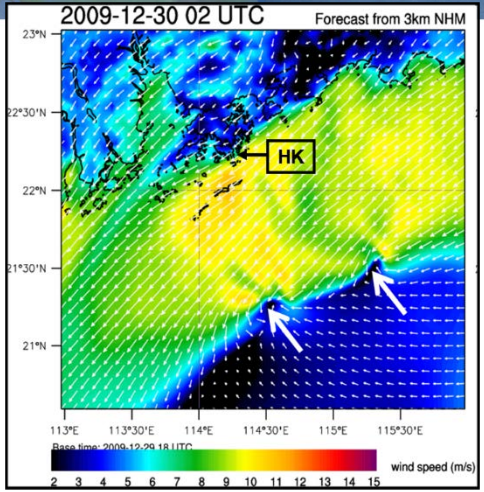

Near-surface wind vectors and wind speed (colour coding) calculated with the AIR model of the Hong Kong Observatory with 3 km resolution for 30-12-2009 ,0200 UTC (1000 LT). Note the two notches in the frontal line marked by arrows.

Model rainfall

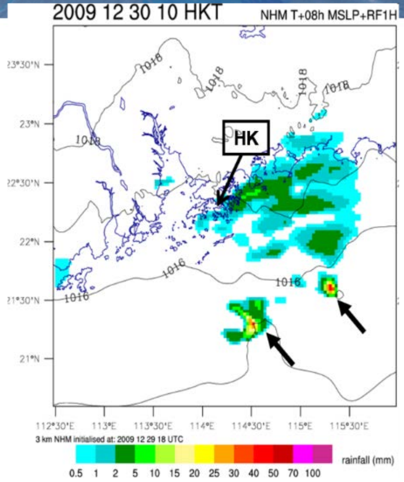

1-hour accumulated rainfall (colour shading) calculated with the AIR model with 3 km resolution for 30-12-2009 , 0200 UTC (1000 LT) Note the two distinct rain cells marked by arrows which are located at the positions where the frontal boundary has notches.

Wind front east of Taiwan

generated by airflow reflected by a mountain chain

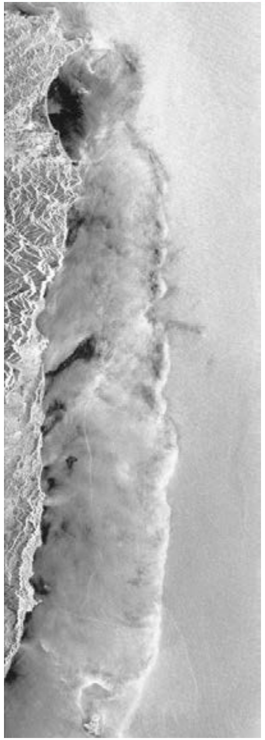

ERS-2 SAR,
18-1-1999

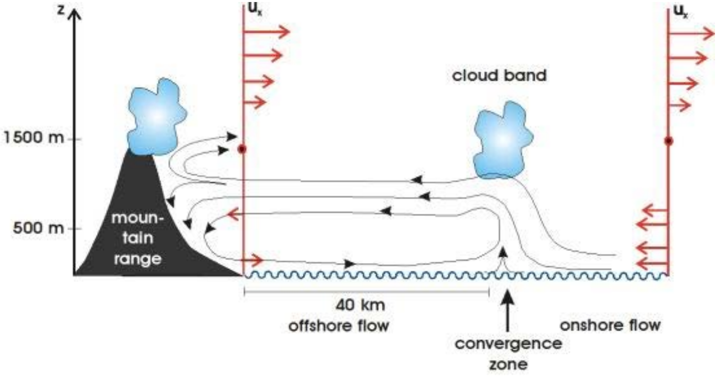

Sketch of the airflow

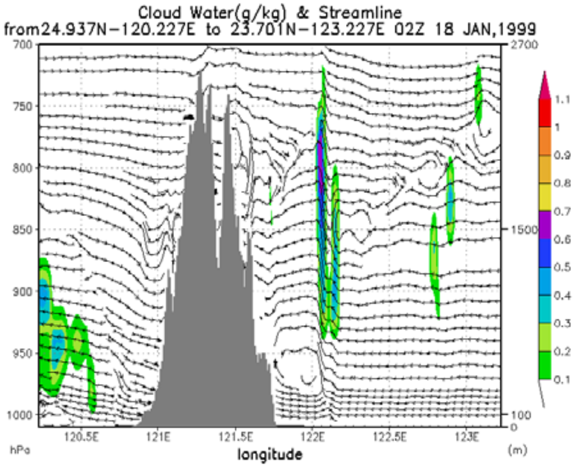

Model results obtained from the MM 5 model

Cloud water and streamlines

Multi-sensor analysis of a wind front east of Taiwan

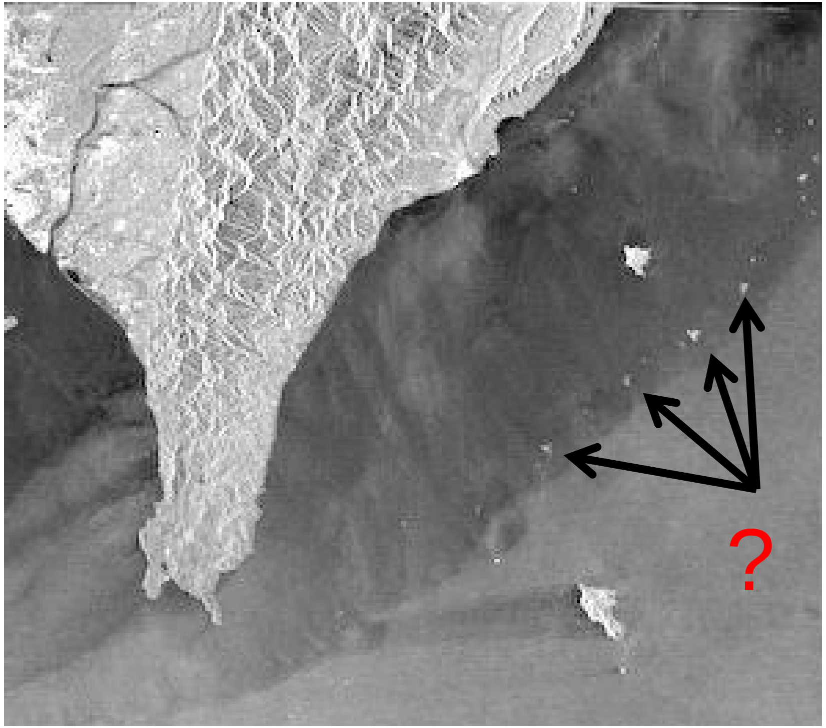

Envisat ASAR WS image,11-12-2006,1403 UTC

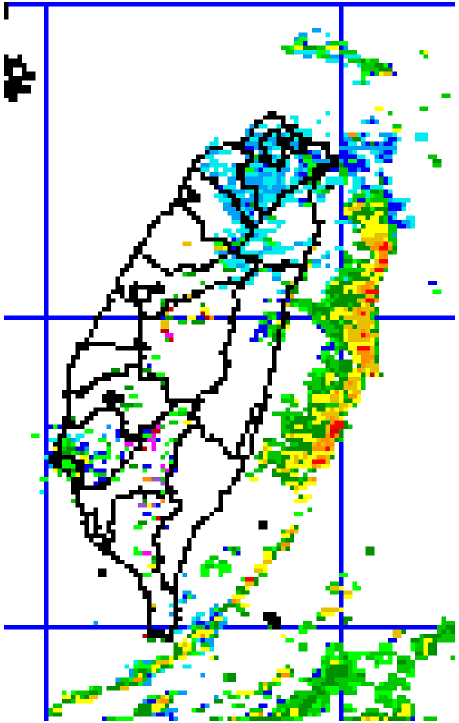

Weather radar image,
11 Dec. 2006, 14:00 UTC

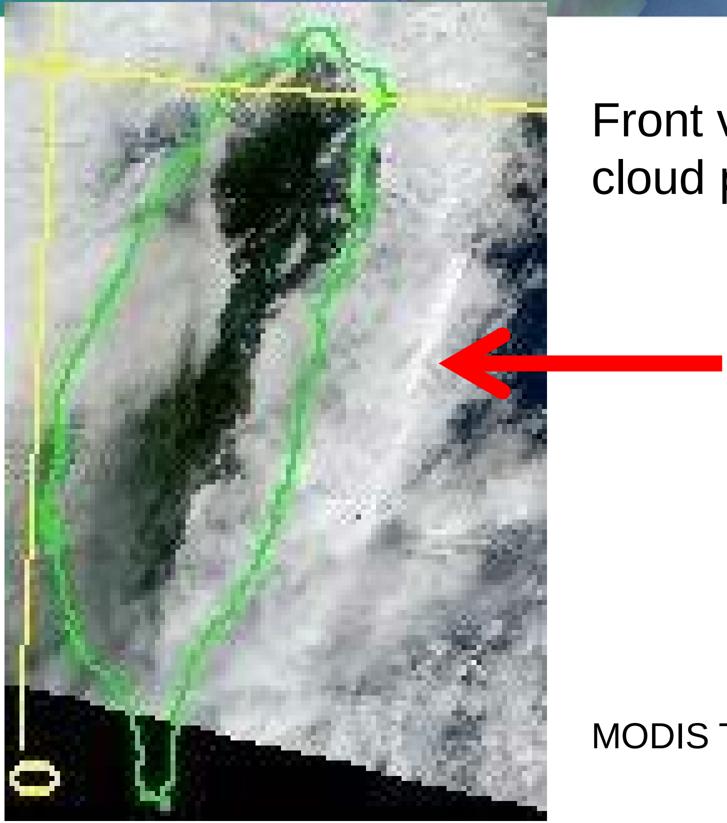

Front visible in the cloud pattern

MODIS Terra image , 12-12-2006, 02:15 UTC

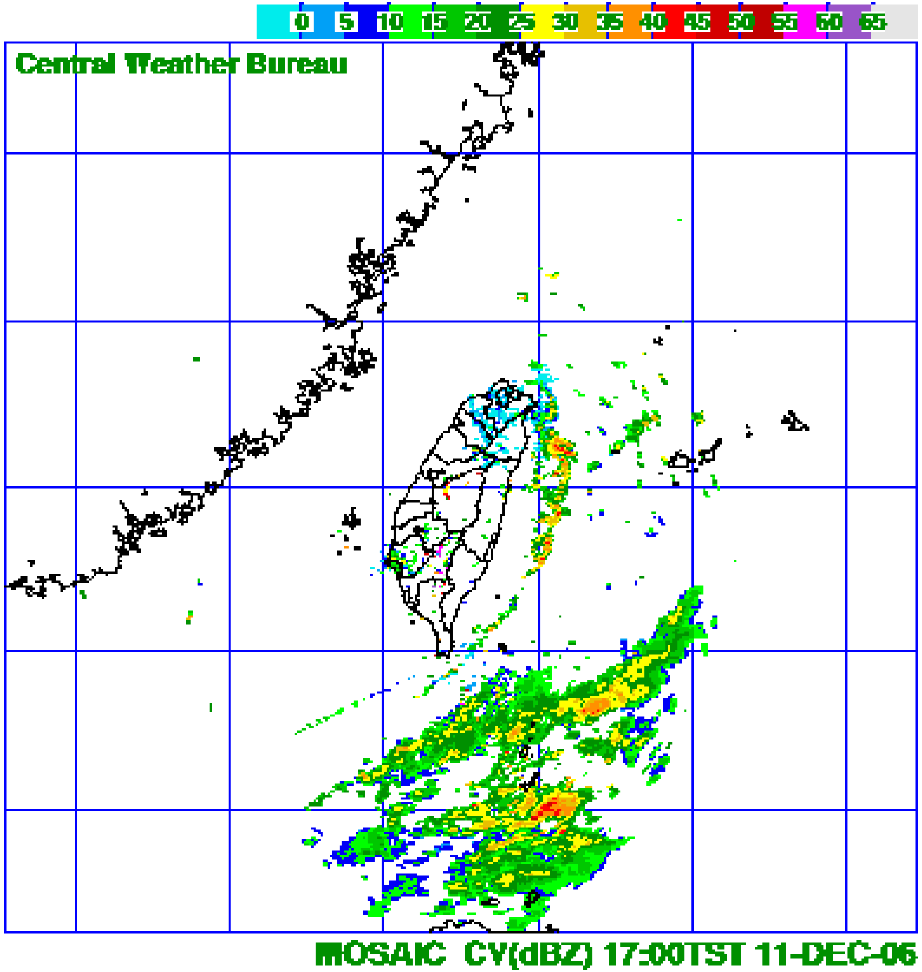

11 Dec 2006
17:00 TST

↓

12 Dec 2006
15:00 TST

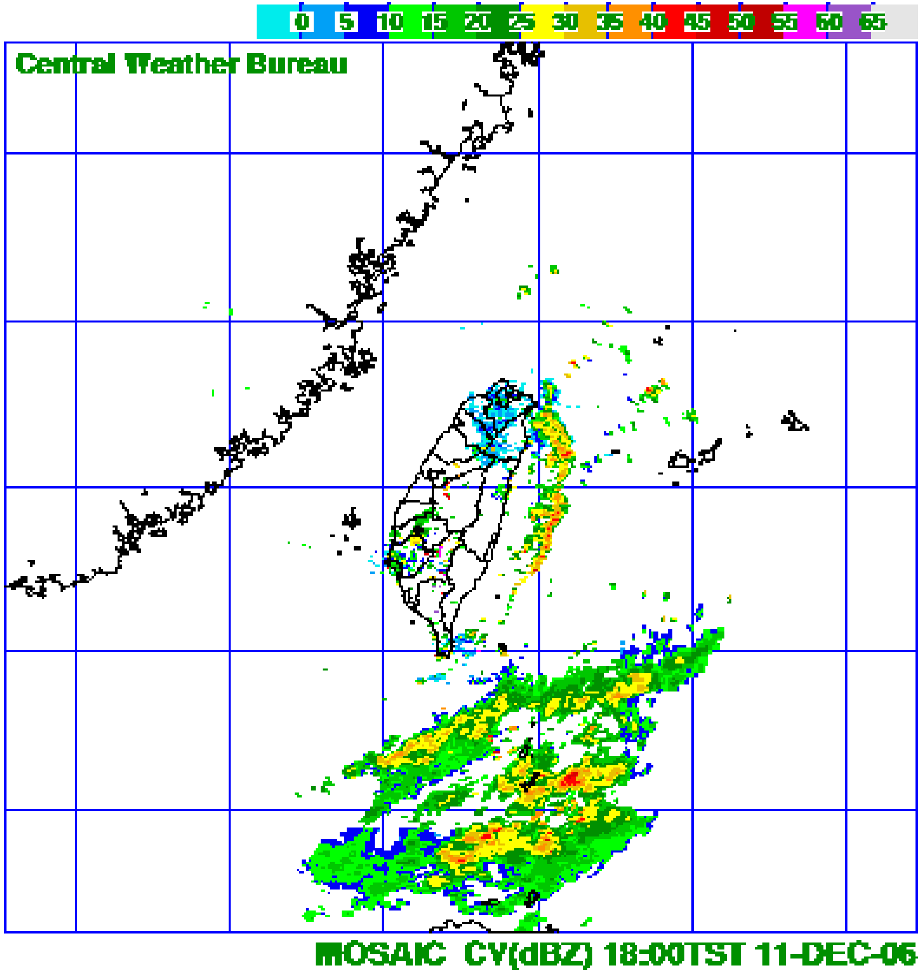

11 Dec 2006
17:00 TST

↓

12 Dec 2006
15:00 TST

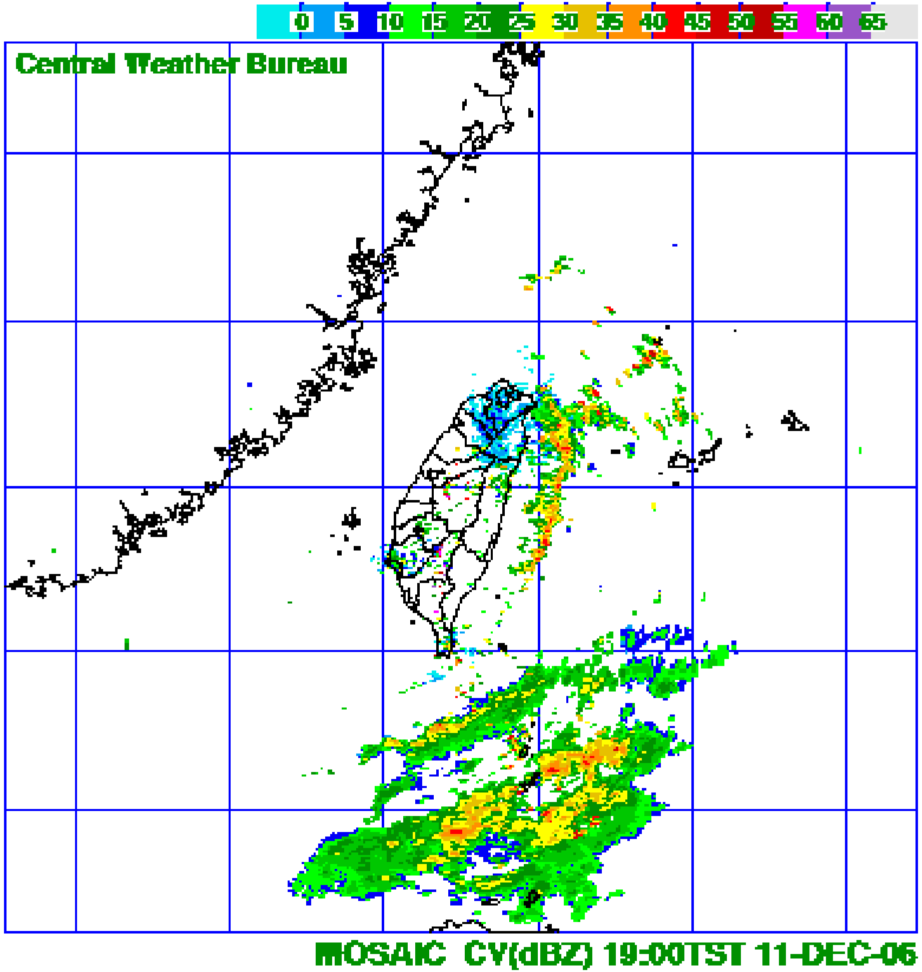

11 Dec 2006
17:00 TST

↓

12 Dec 2006
15:00 TST

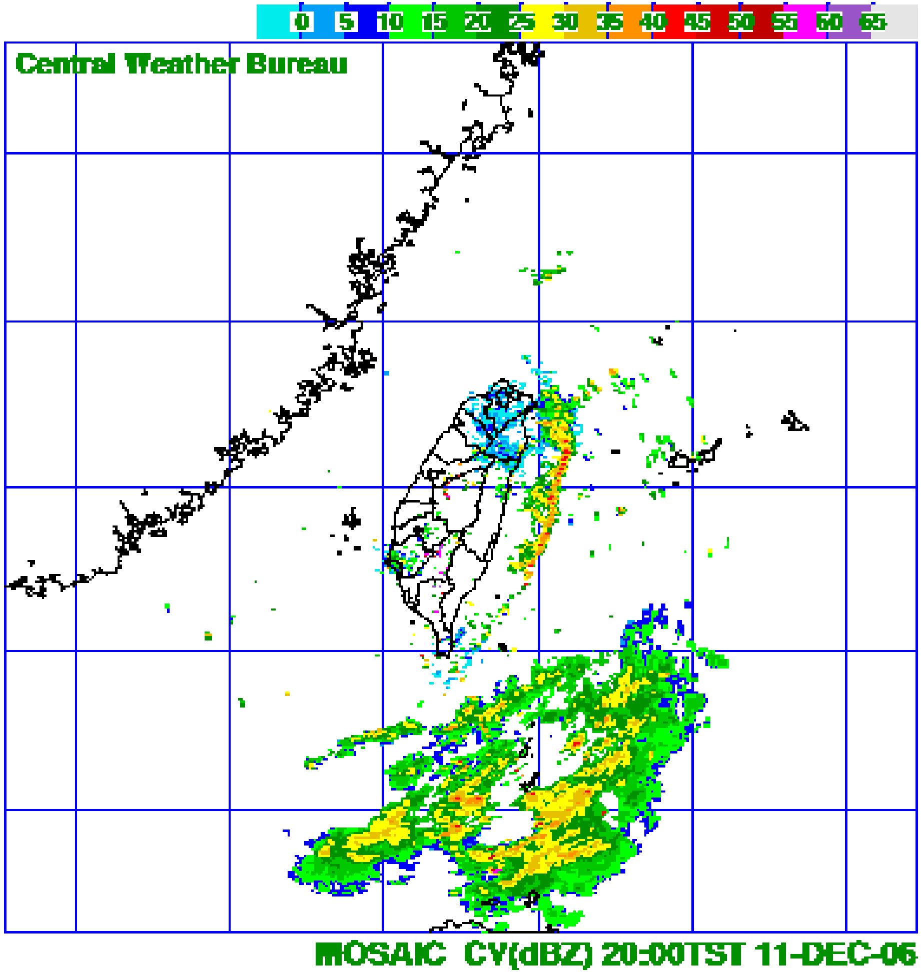

11 Dec 2006
17:00 TST

↓

12 Dec 2006
15:00 TST

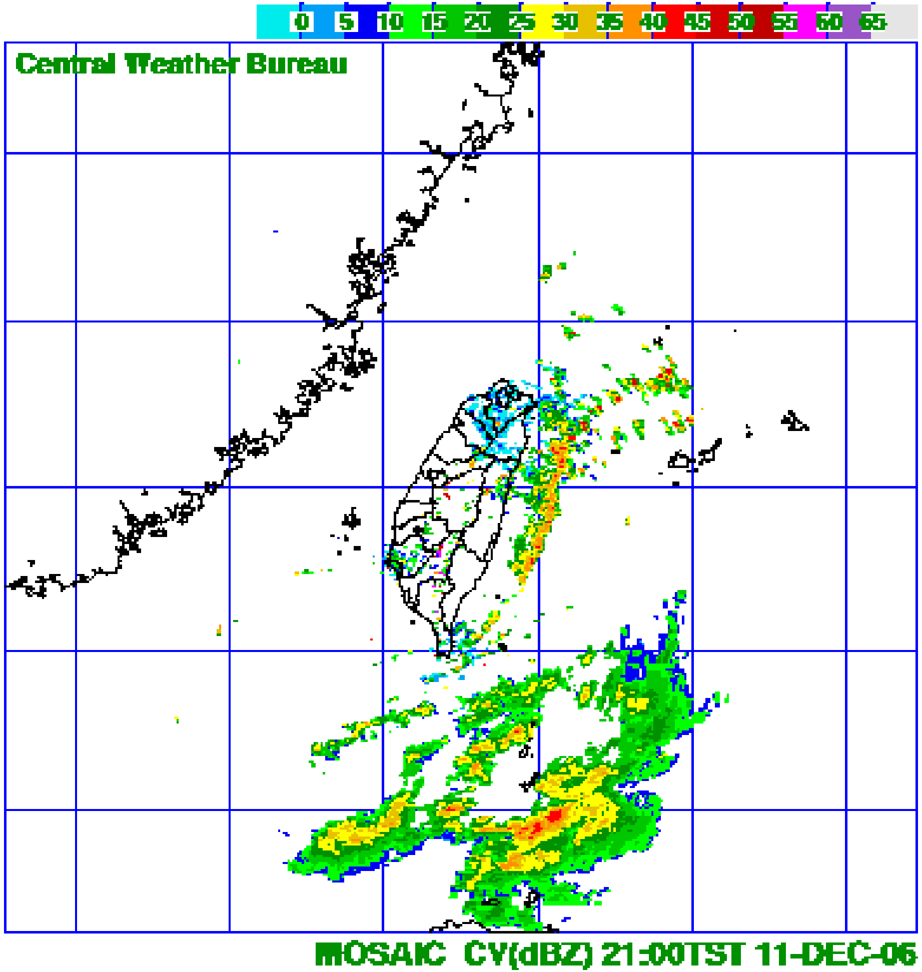

11 Dec 2006
17:00 TST

↓

12 Dec 2006
15:00 TST

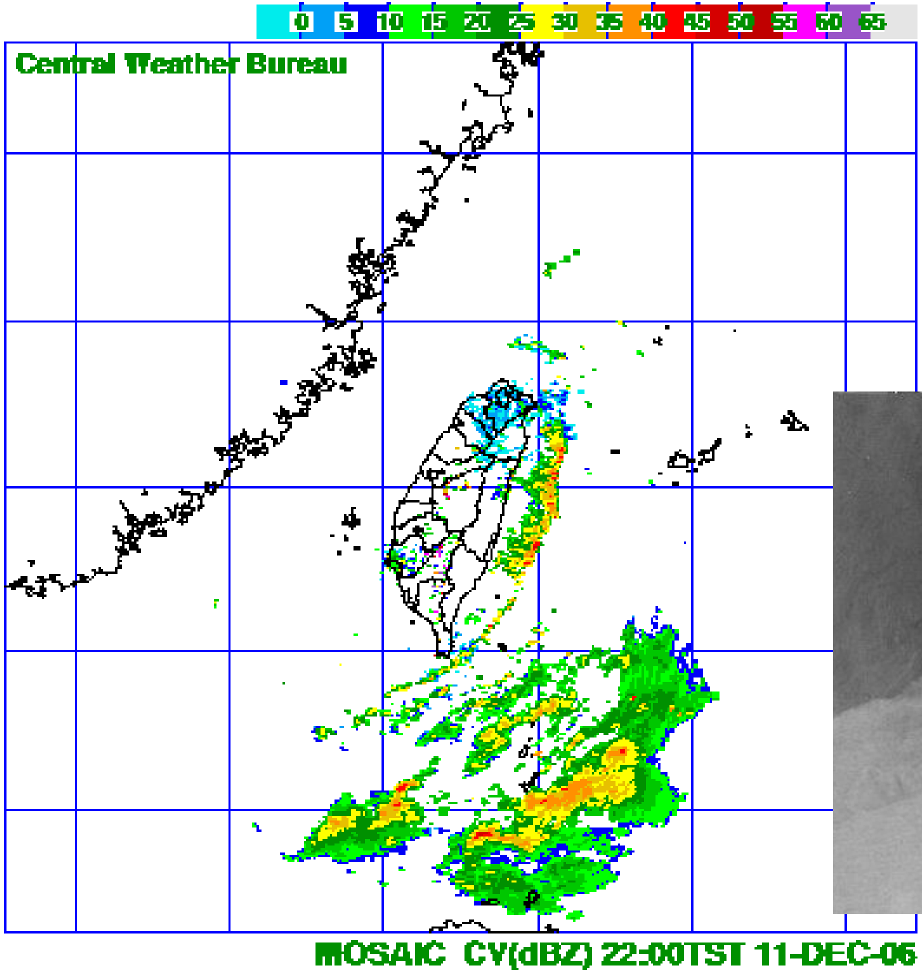

11 Dec 2006
17:00 TST

12 Dec 2006
15:00 TST

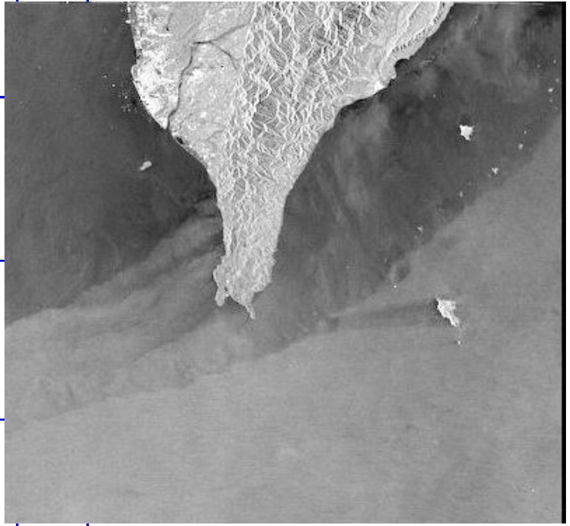

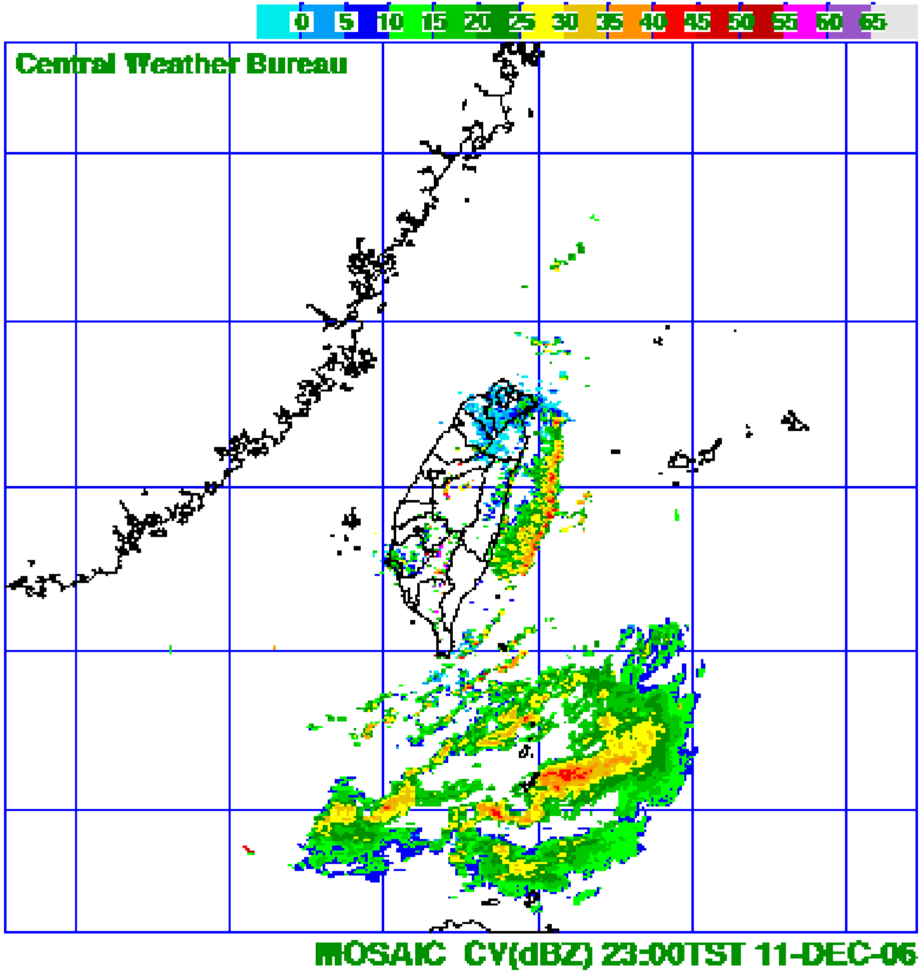

11 Dec 2006
17:00 TST

↓

12 Dec 2006
15:00 TST

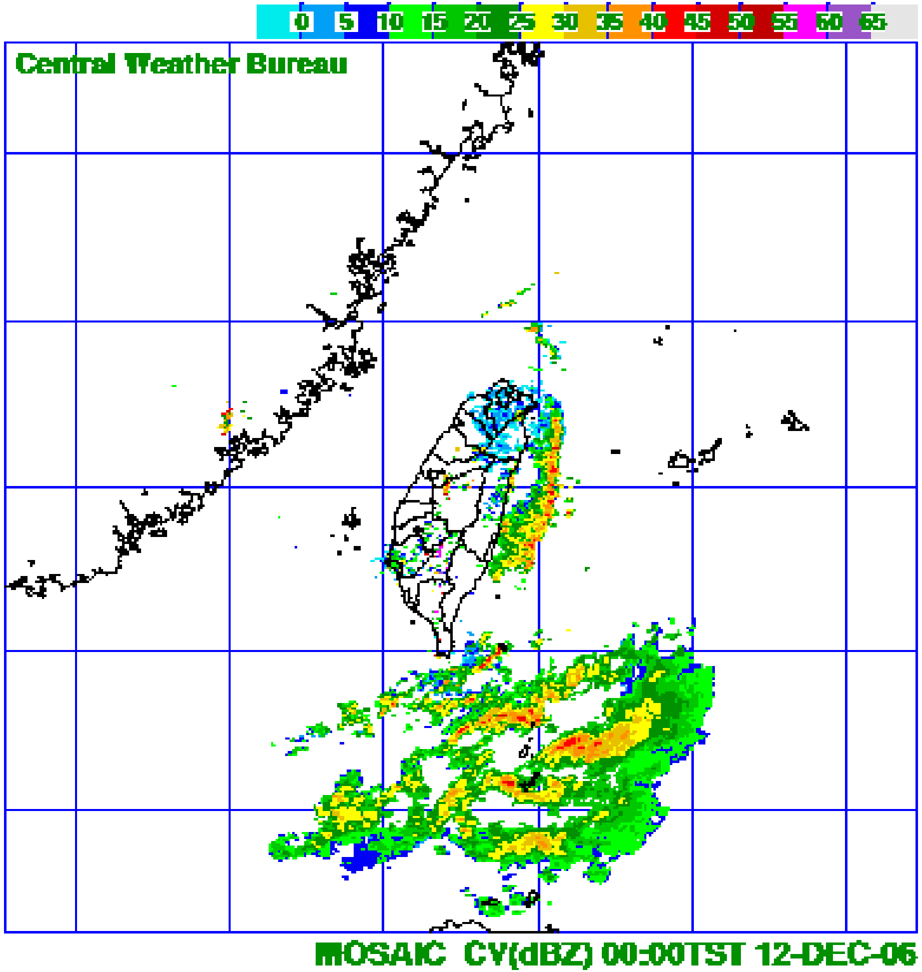

11 Dec 2006
17:00 TST

↓

12 Dec 2006
15:00 TST

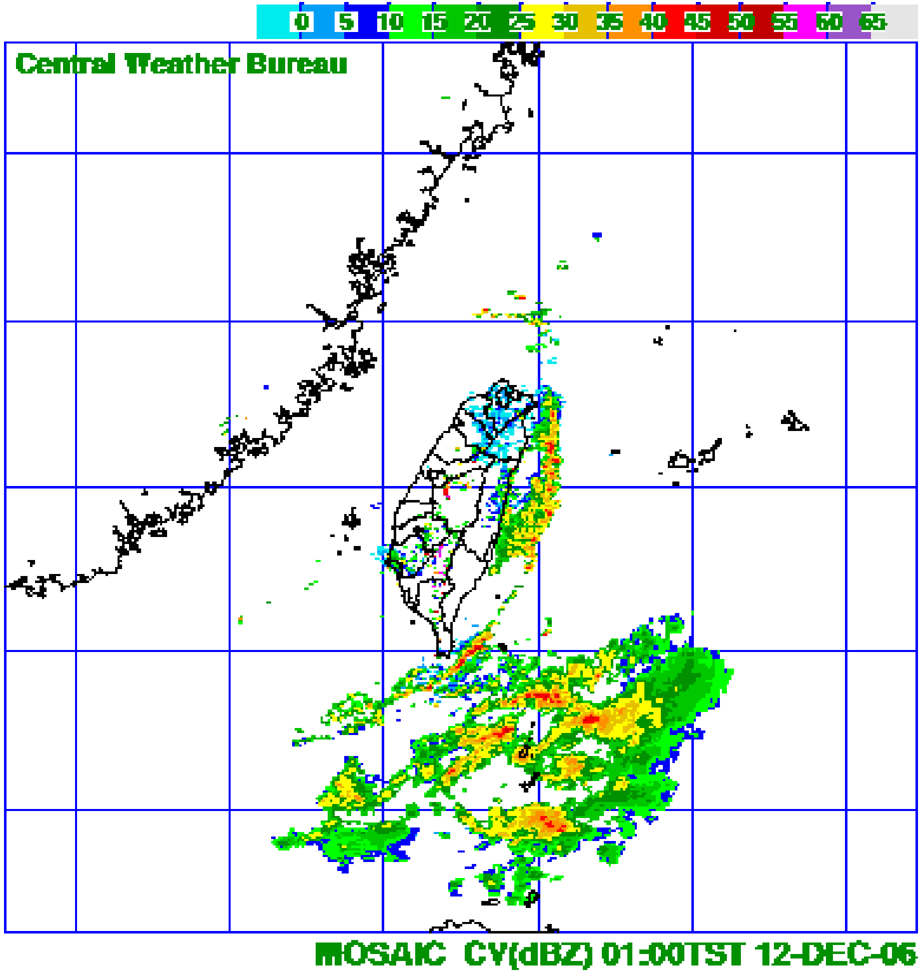

11 Dec 2006
17:00 TST

↓

12 Dec 2006
15:00 TST

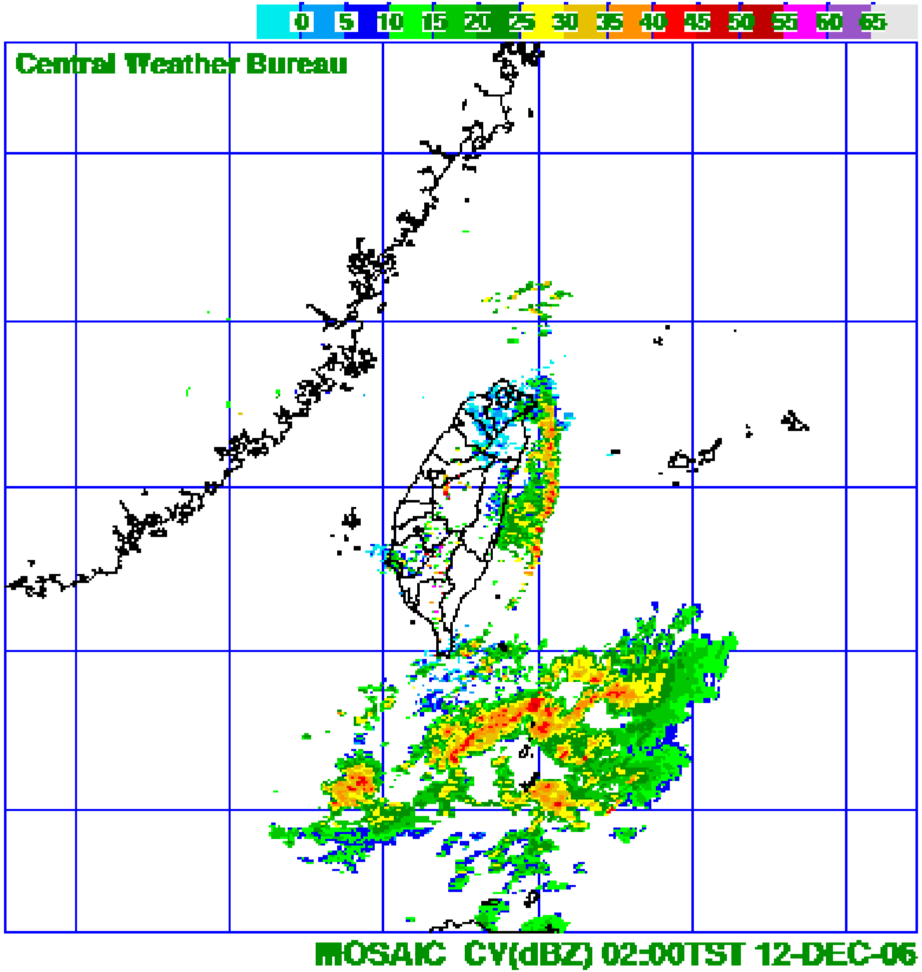

11 Dec 2006
17:00 TST

↓

12 Dec 2006
15:00 TST

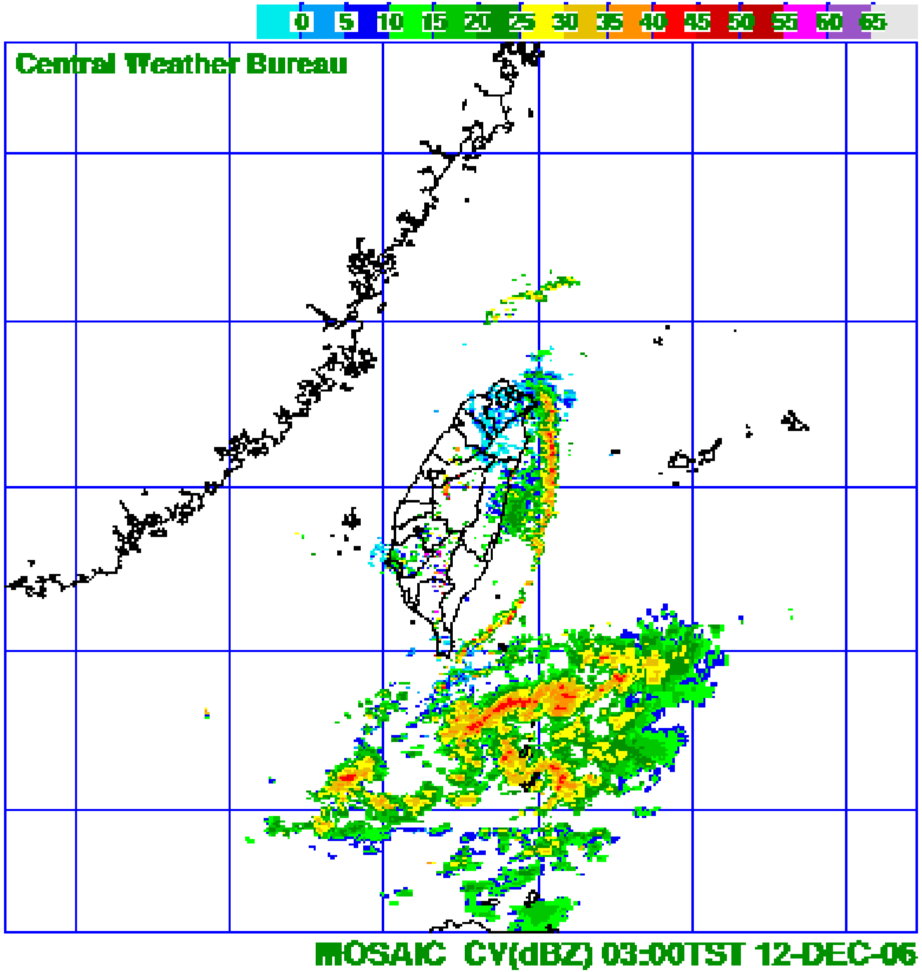

11 Dec 2006
17:00 TST

↓

12 Dec 2006
15:00 TST

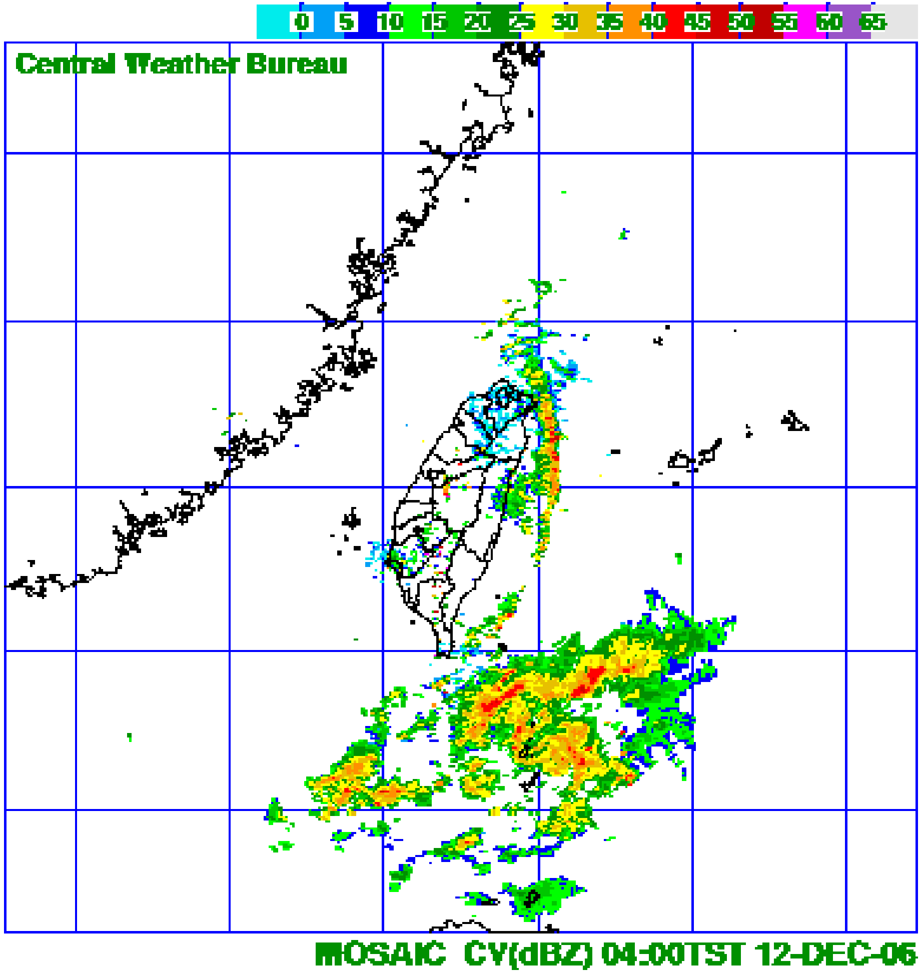

11 Dec 2006
17:00 TST

↓

12 Dec 2006
15:00 TST

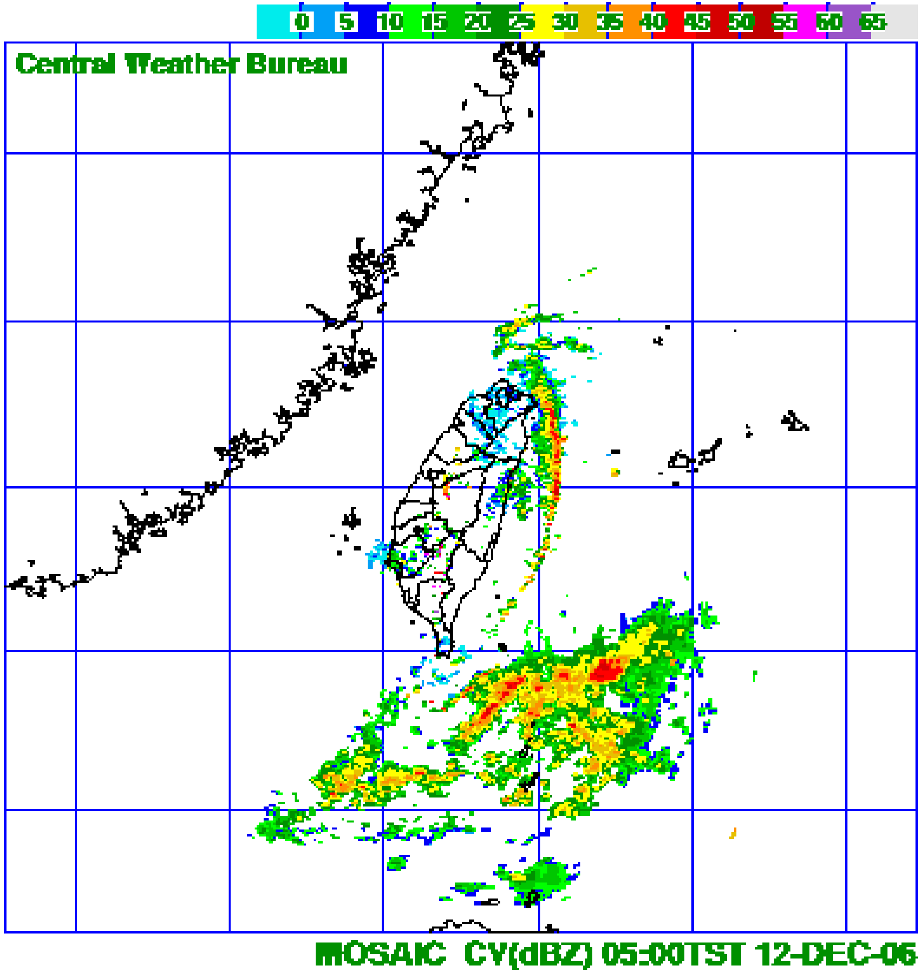

11 Dec 2006
17:00 TST

↓

12 Dec 2006
15:00 TST

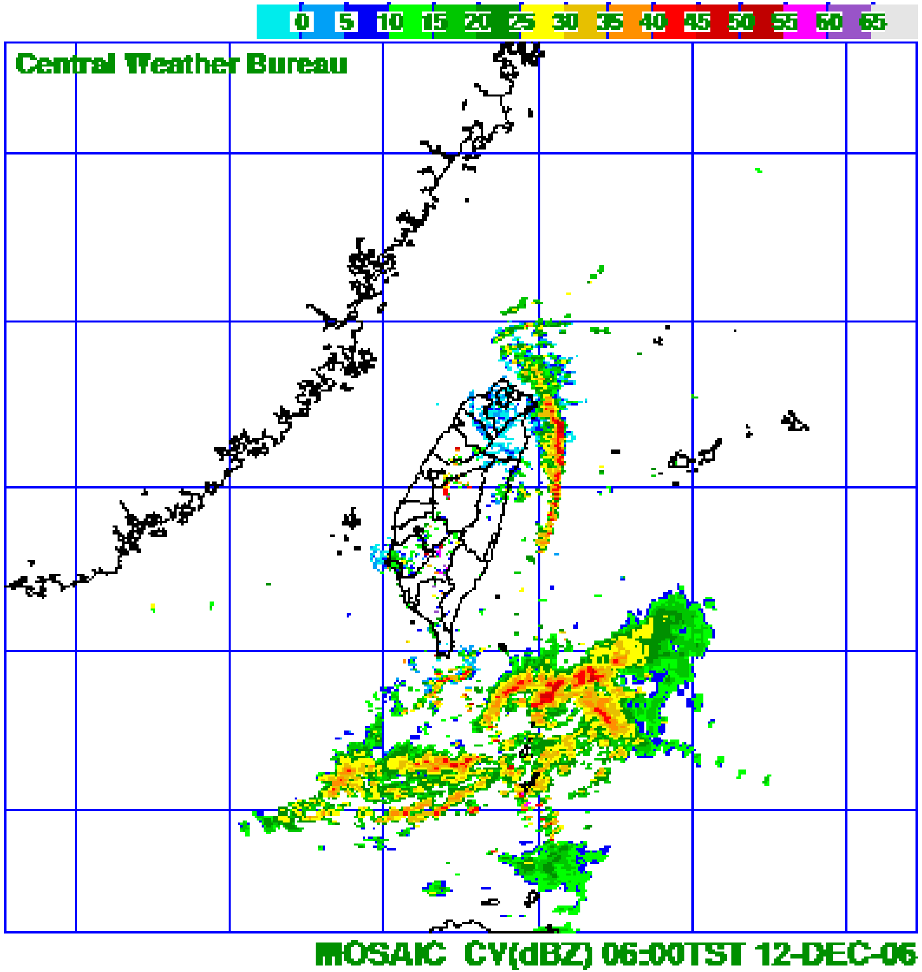

11 Dec 2006
17:00 TST

↓

12 Dec 2006
15:00 TST

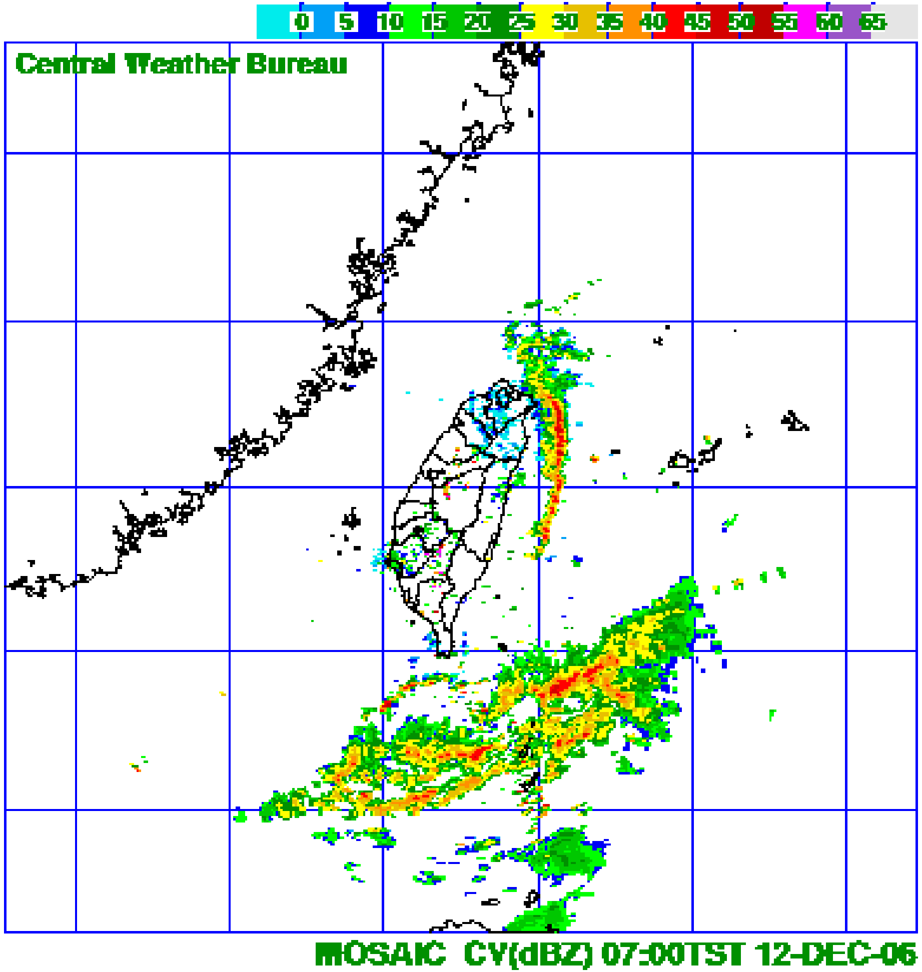

11 Dec 2006
17:00 TST

↓

12 Dec 2006
15:00 TST

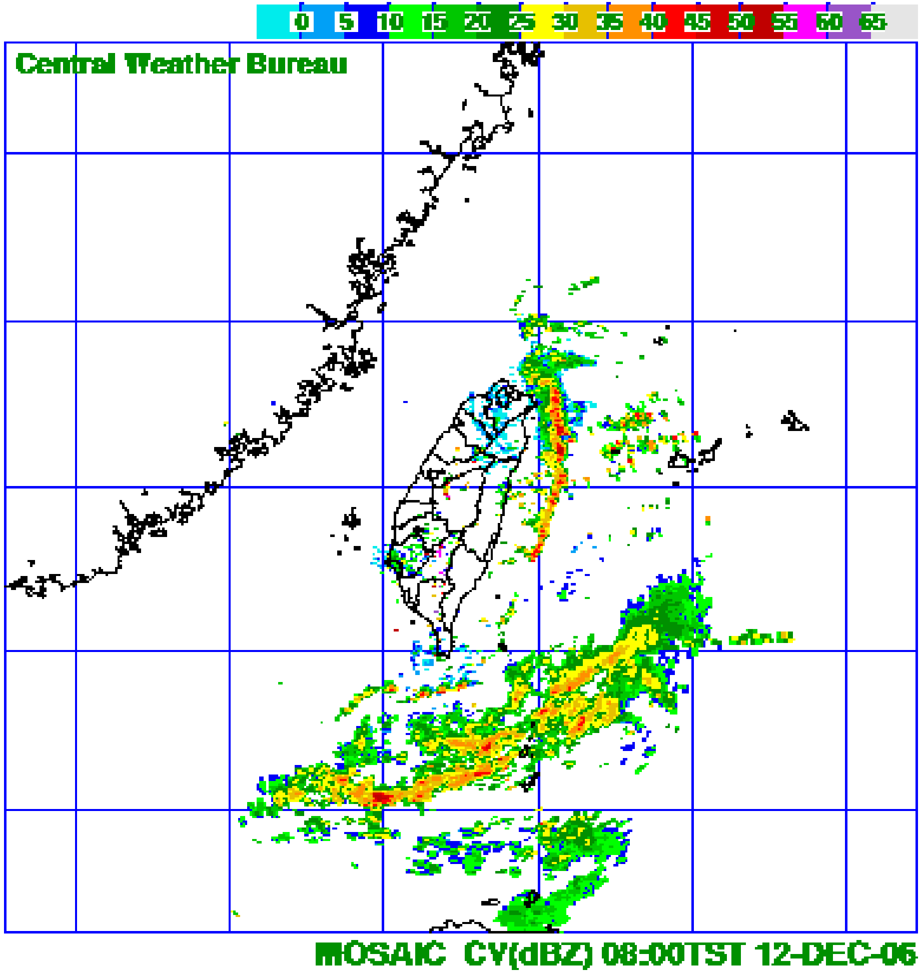

11 Dec 2006
17:00 TST

12 Dec 2006
15:00 TST

11 Dec 2006
17:00 TST

↓

12 Dec 2006
15:00 TST

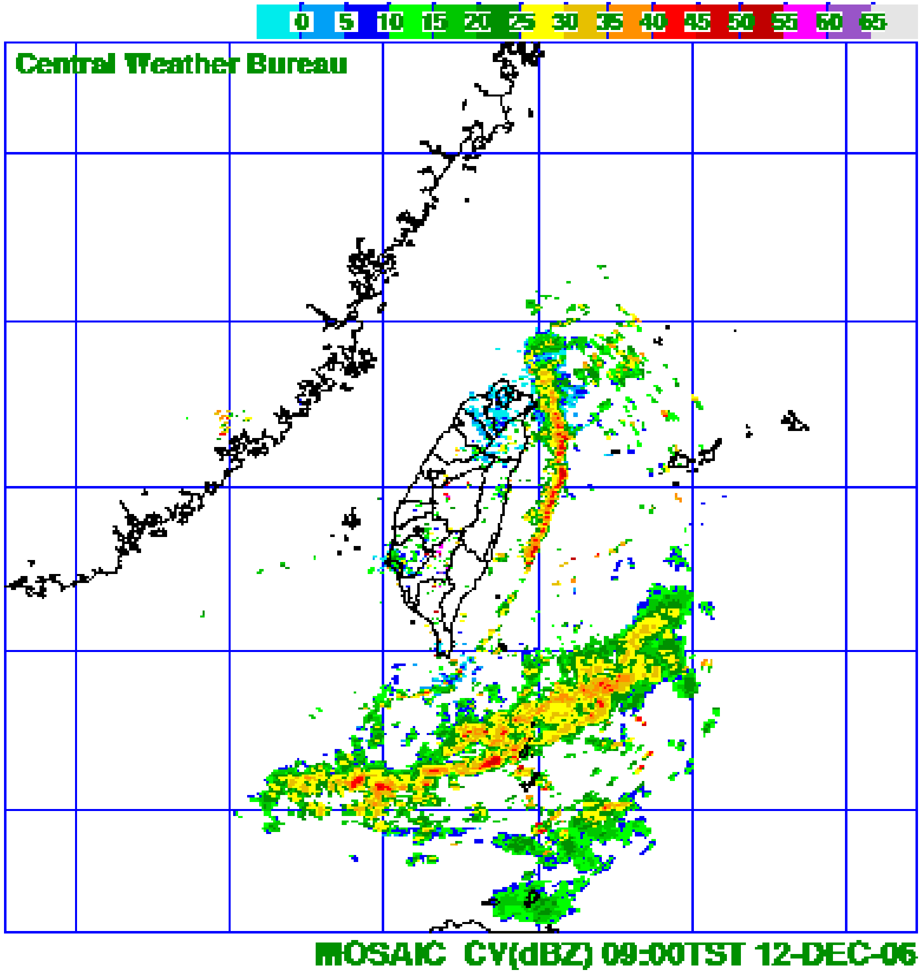

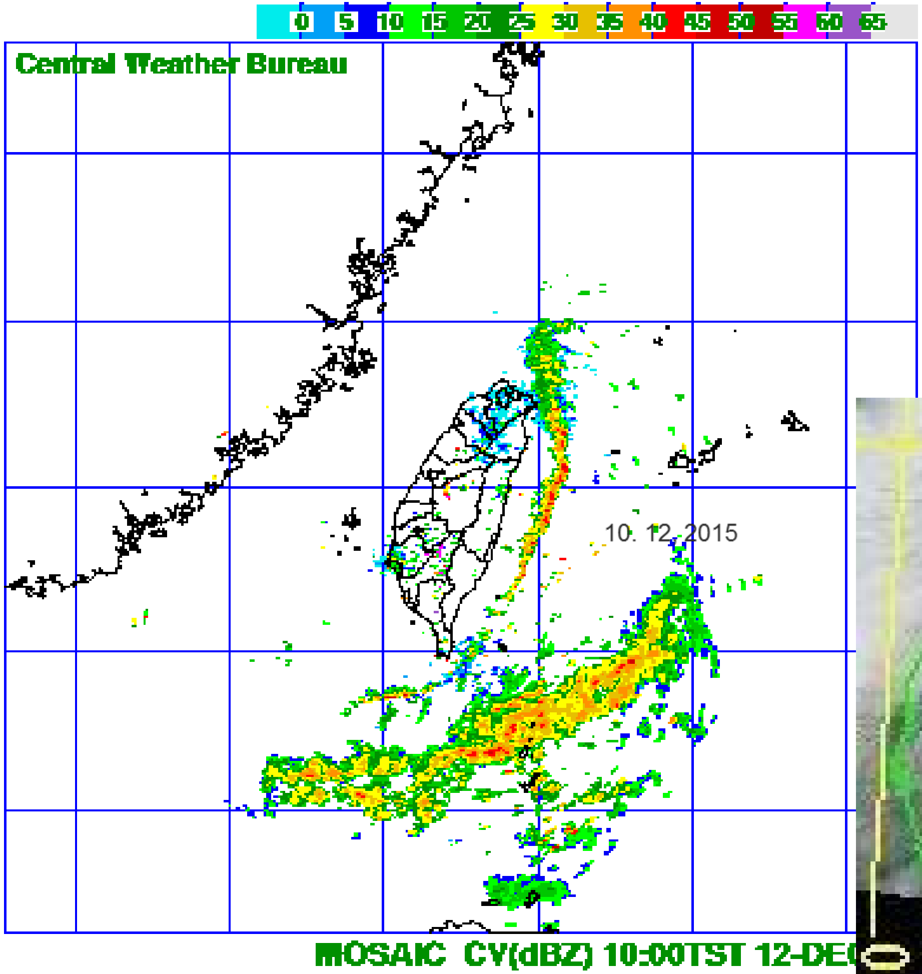

11 Dec 2006
17:00 TST

↓

12 Dec 2006
15:00 TST

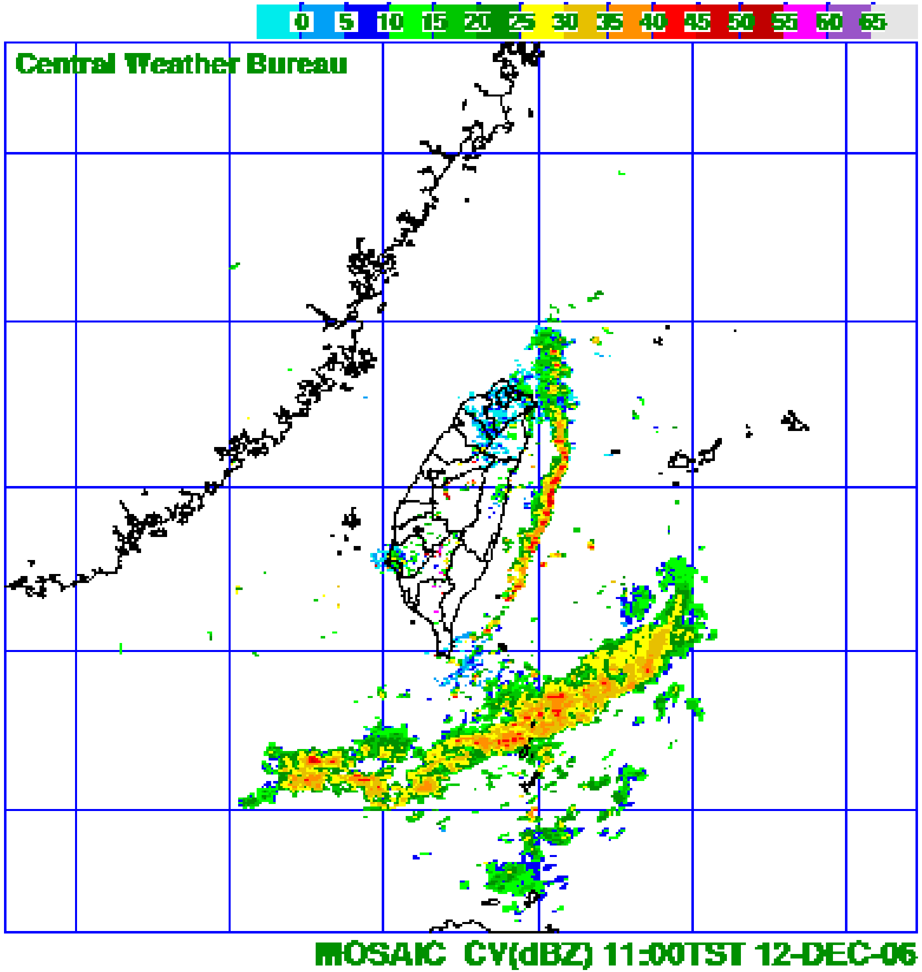

11 Dec 2006
17:00 TST

↓

12 Dec 2006
15:00 TST

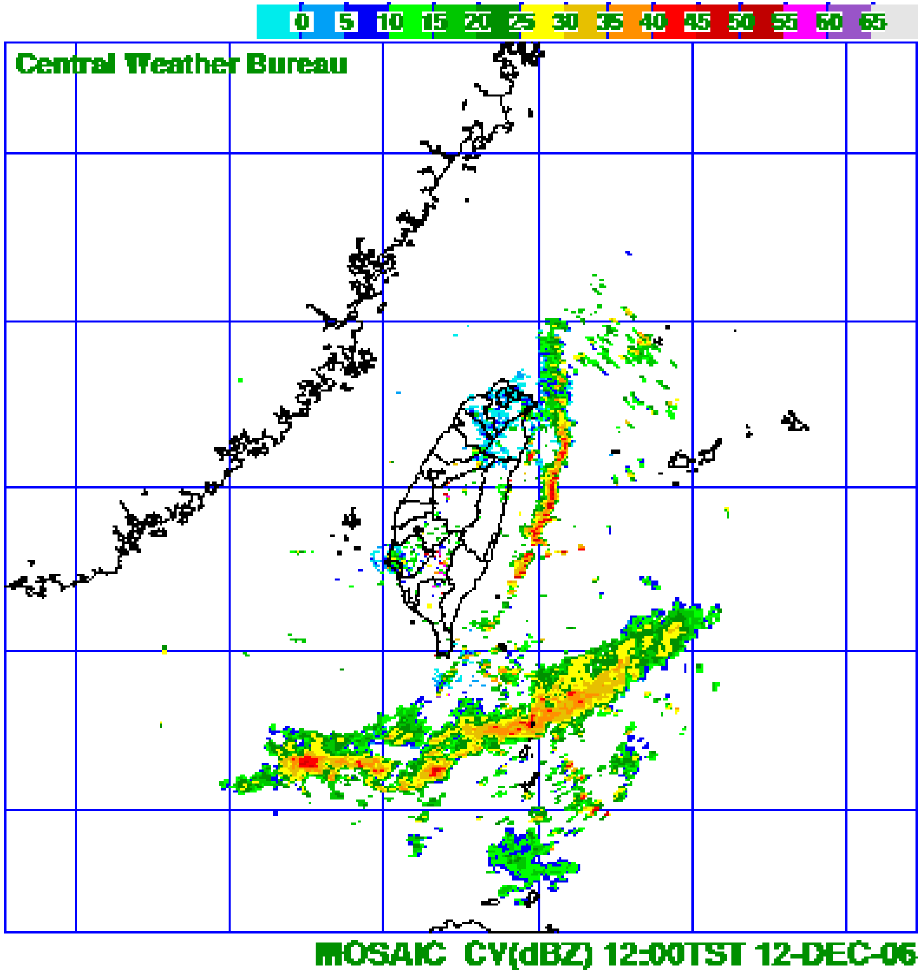

11 Dec 2006
17:00 TST

12 Dec 2006
15:00 TST

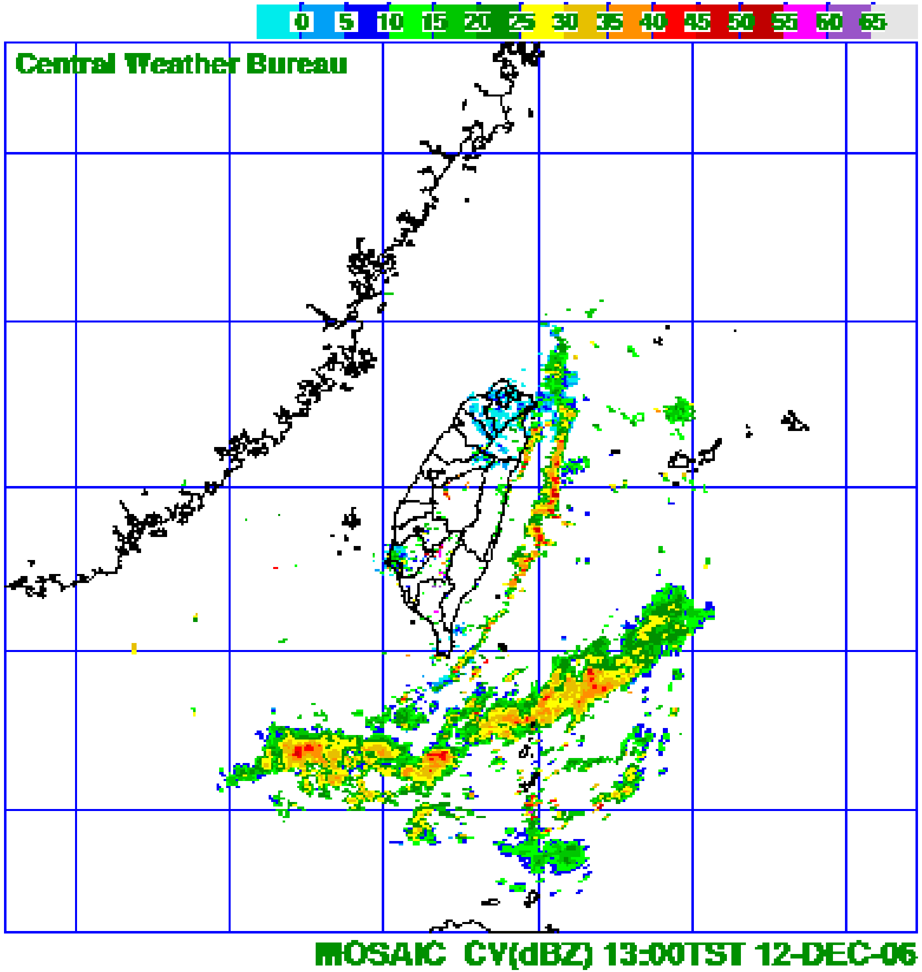

11 Dec 2006
17:00 TST

12 Dec 2006
15:00 TST

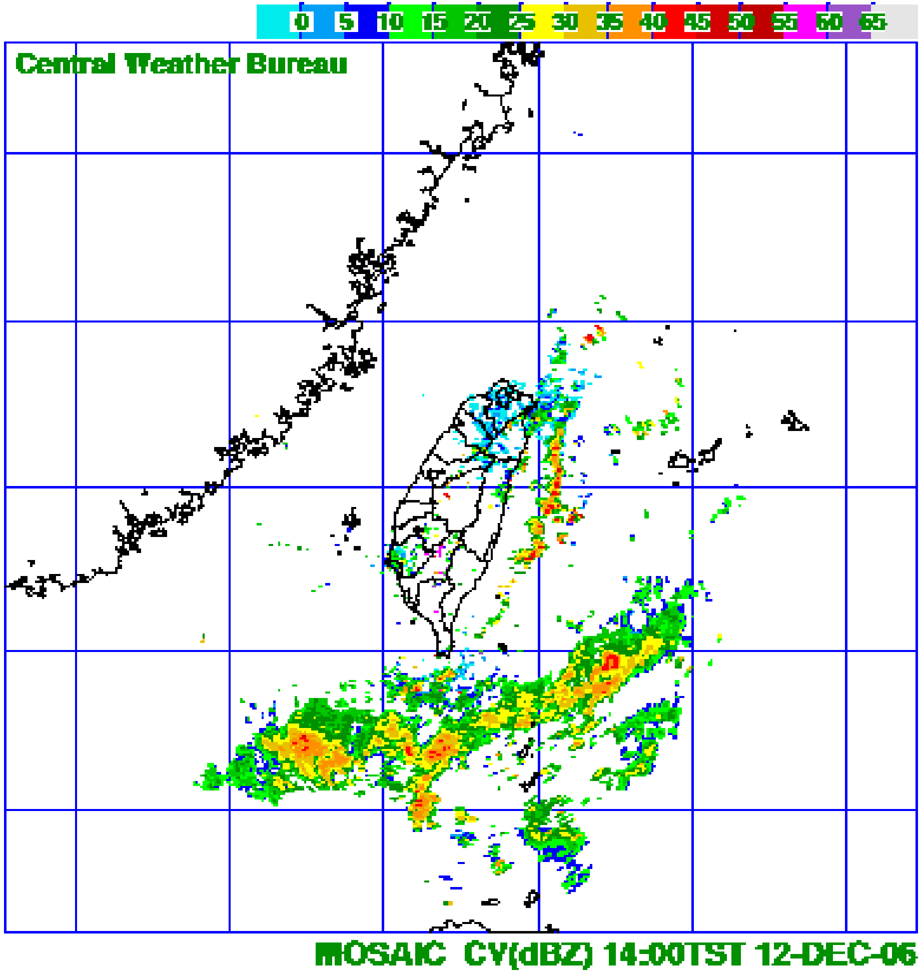

11 Dec 2006
17:00 TST

↓

12 Dec 2006
15:00 TST

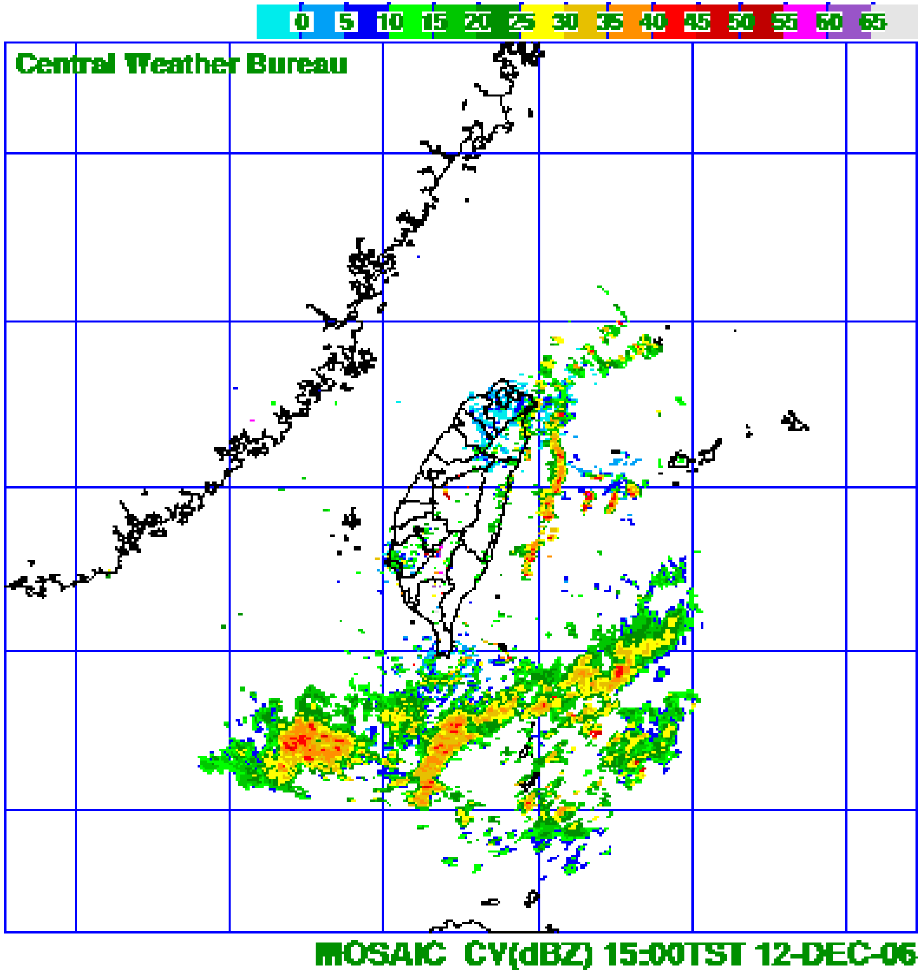

11 Dec 2006
17:00 TST

↓

12 Dec 2006
15:00 TST

Atmospheric gravity waves

1) Generated by interaction of stratified airflow with a mountain range (lee waves)

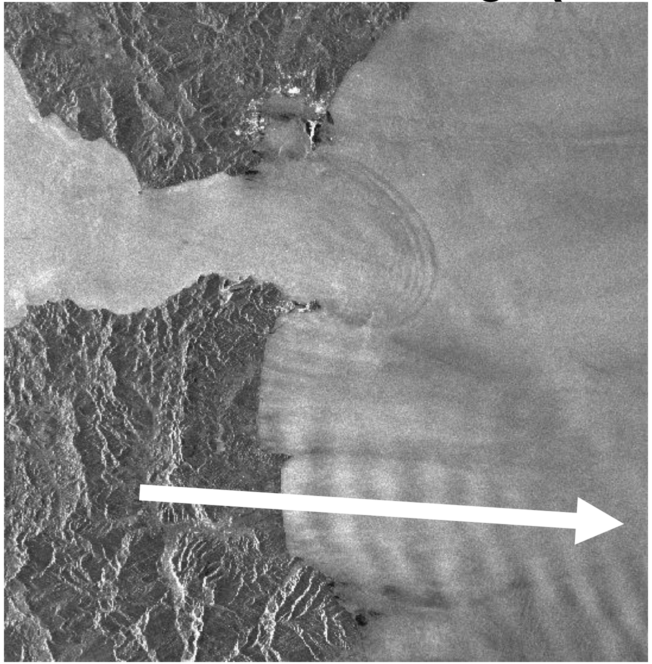

Strait of Gibraltar

ERS-1 SAR, 03-09-1993, 22:39 UTC; imaged area: 100 km x 100 km.

Sketch of the generation of an atmospheric gravity wave (lee wave) behind a mountain range.

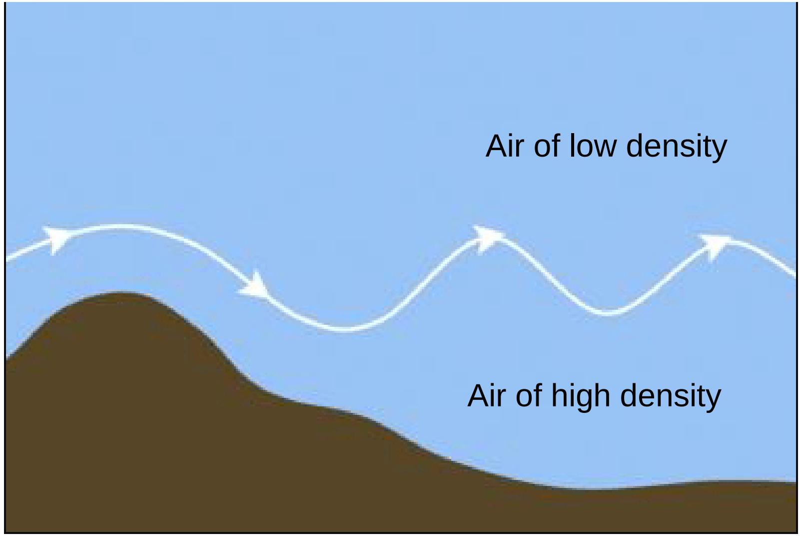

The COMET Program

Nonlinear atmospheric gravity waves behind a mountain (lee waves)

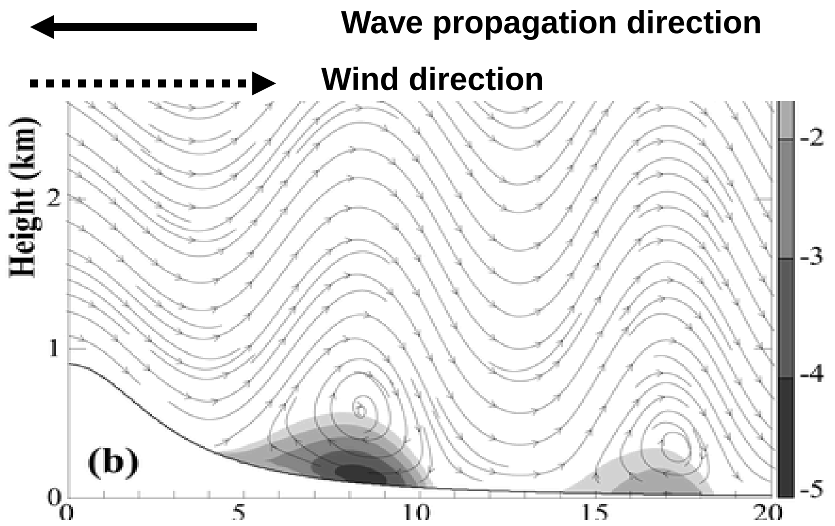

Drawn are the the streamlines of secondary flow plus background flow

Wind speed variation caused by the atmospheric gravity wave

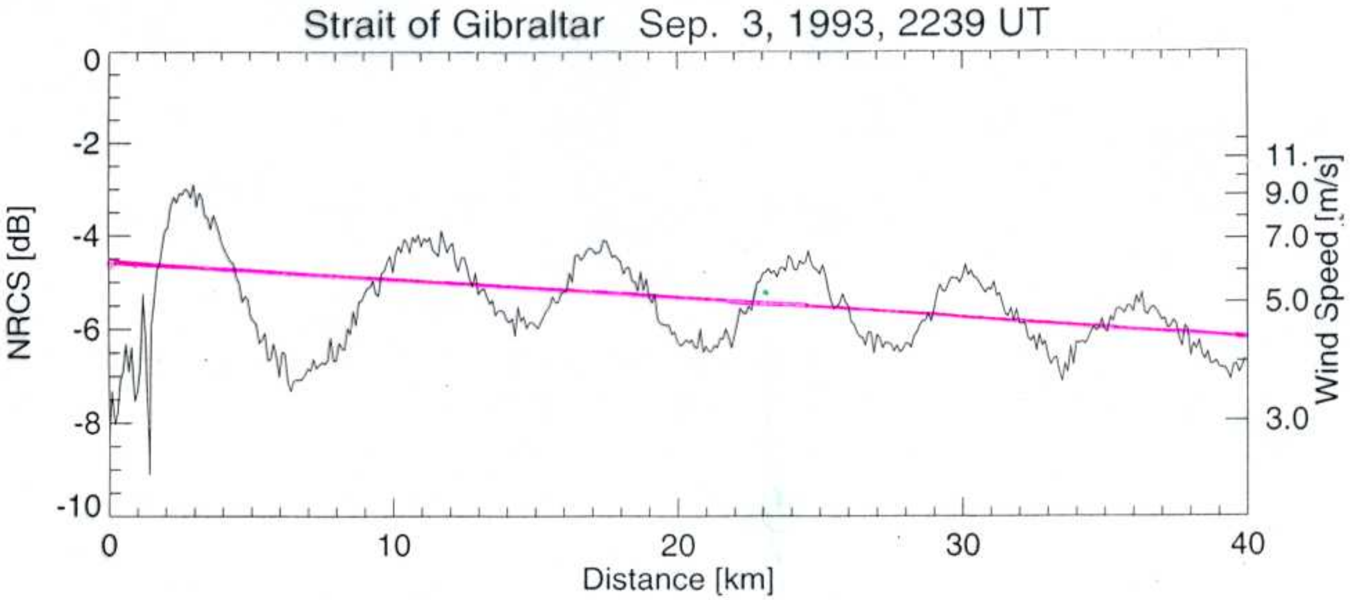

Image intensity scan from west to east through the internal lee wave pattern east of the Maroccan coast is shown in the previous figure. On the left-hand vertical coordinate axis the normalized radar cross section (NRCS) is plotted and on the right-hand vertical coordinate axis the wind speed at a height of 10 m above sea level as calculated from the wind scatterometer model CMOD4.

2) generated by wind shear

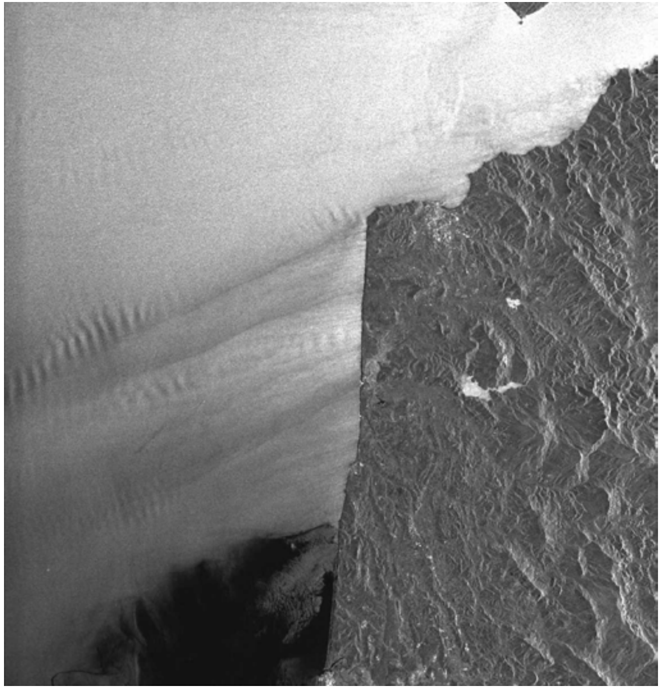

West coast of Morocco, Strait og Gibraltar

ERS-1 SAR image acquired on 06 June 2000 at 11:05 UTC; imaged area: 100 km x 100 km.

It is often not easy to decide whether wave patterns visible on SAR images of the sea surface are sea surface signatuures of oceanic internal waves or of atmospheric gravity waves (AGWs).

Examples of wave patterns visible on SAR images of the sea surface:

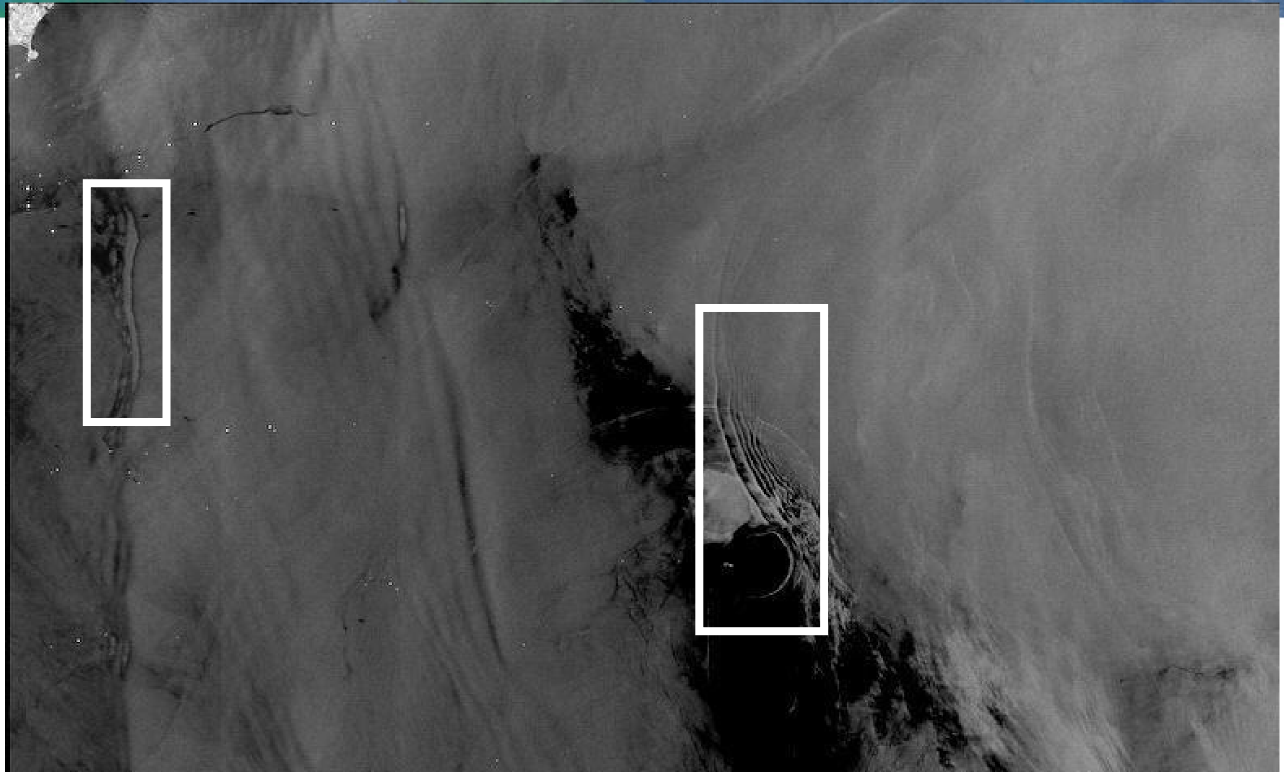


atmospheric


oceanic

SAR imaging of nonlinear atmospheric gravity waves and of nonlinear oceanic internal waves

1) Atmospheric gravity waves

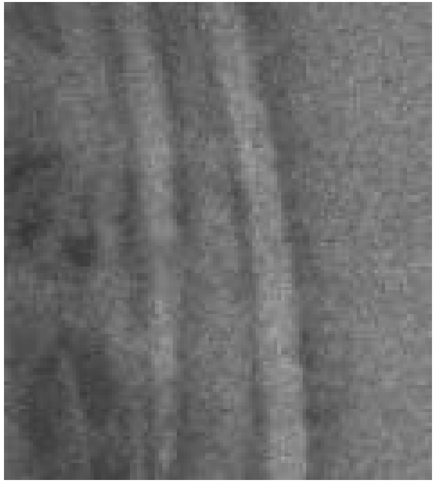

2) Oceanic internal waves

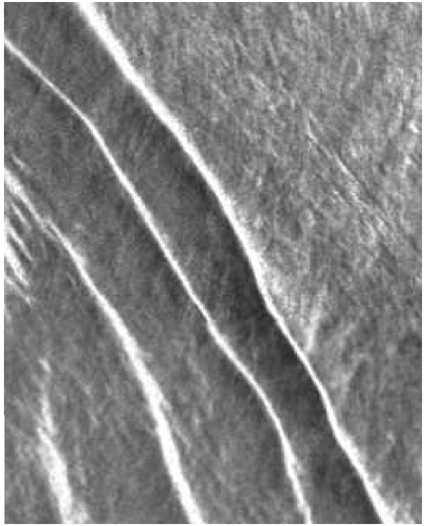

Alpers and Huang, IEEE, TGRS, 2011

Atmospheric boundary layer rolls

Cloud street off the coast of Greenland

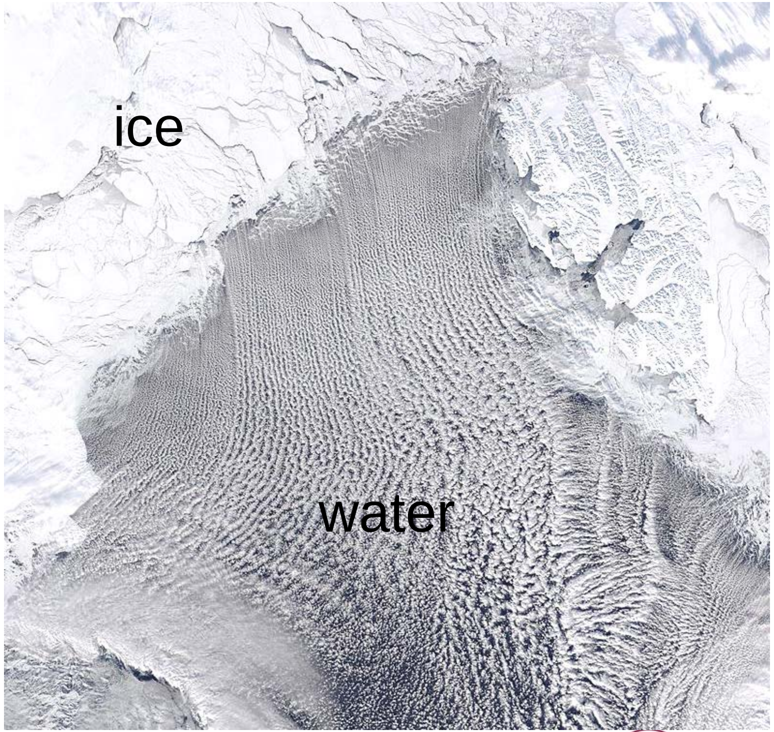

Atmospheric boundary layer rolls are visible in the cloud pattern.

Optical image

Modis Terra image, 29 March 2003 ID: 26012

Atmospheric boundary layer rolls are also visible on SAR images.

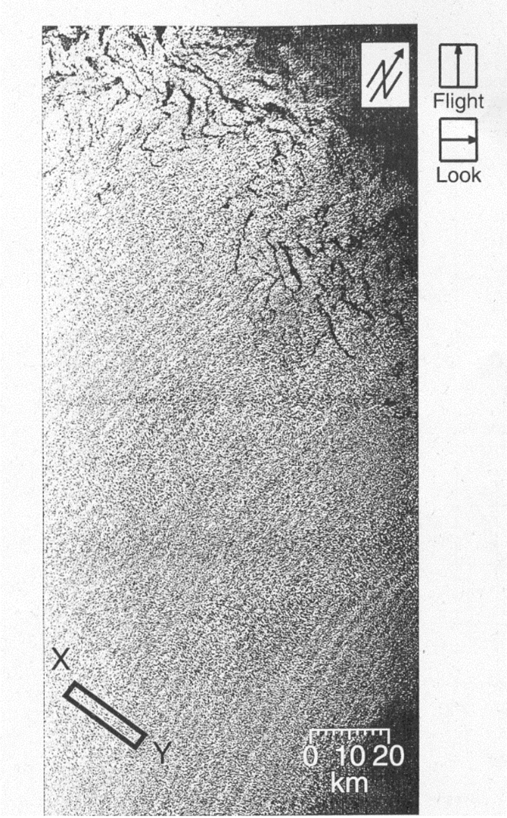

ERS-1 SAR, 24 March 1993, 1954 UTC, Greenland Sea near Spitsbergen

Mueller, G., B. Bruemmer, and W. Alpers: "Roll convection within an arctic cold-air outbreak: Interpretation of in situ aircraft measurements and spaceborne SAR imagery by a three-dimensional atmospheric model", *Monthly Weather Review*, **127**, 363-380, 1999

Air motion associated with atmospheric boundary layer rolls

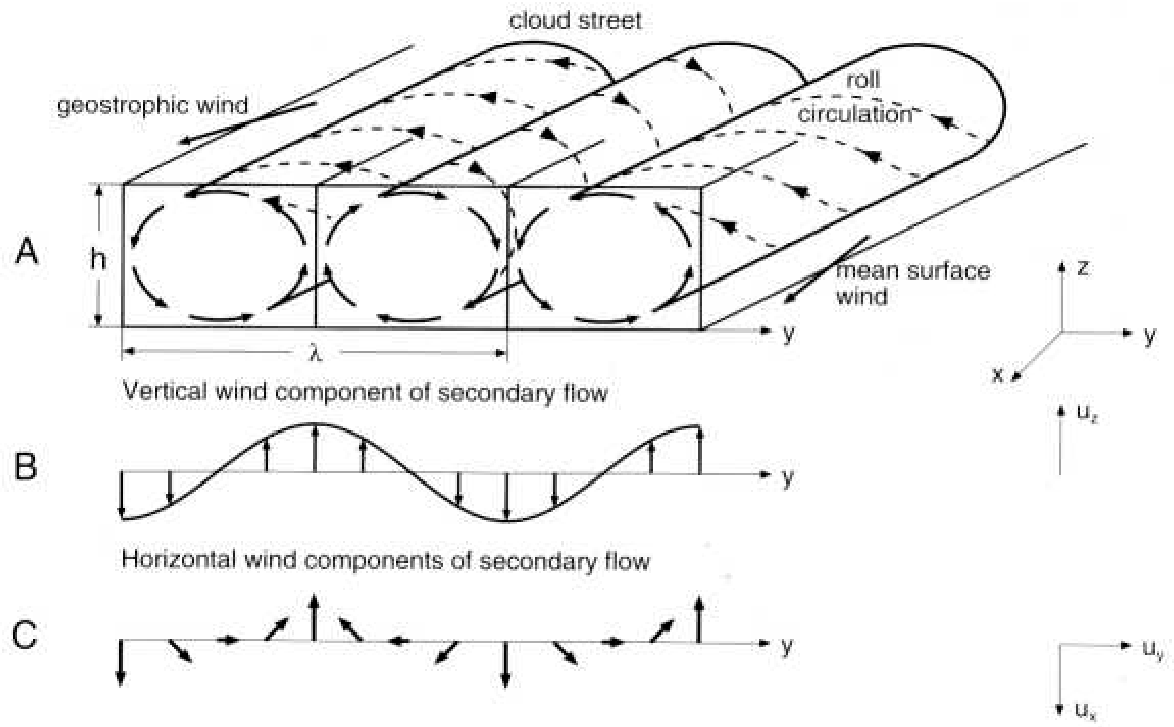

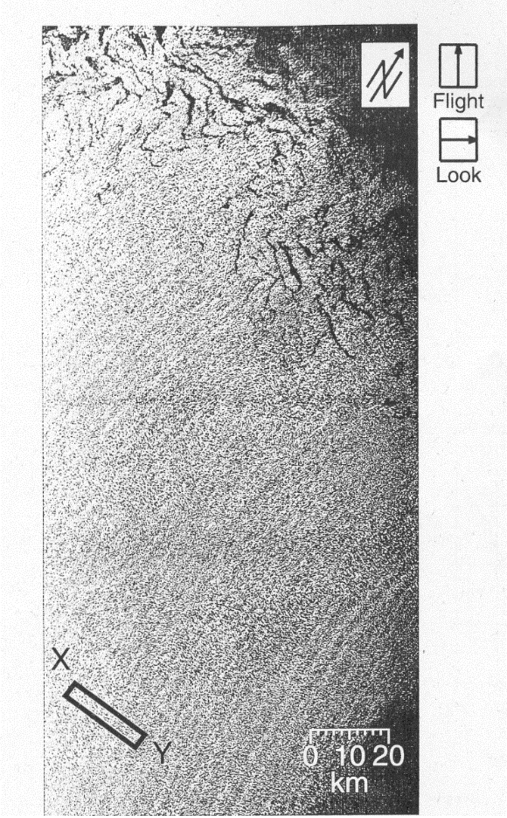

ERS-1 SAR, 24 March 1993, 1954 UTC,
Greenland Sea near Spitsbergen

Mueller, G., B. Bruemmer, and W. Alpers: "Roll convection within an arctic cold-air outbreak: Interpretation of in situ aircraft measurements and spaceborne SAR imagery by a three-dimensional atmospheric model", *Monthly Weather Review*, **127**, 363-380, 1999

Mean variation of the NRCS in dB derived from the scans in the framed area of the ERS SAR image

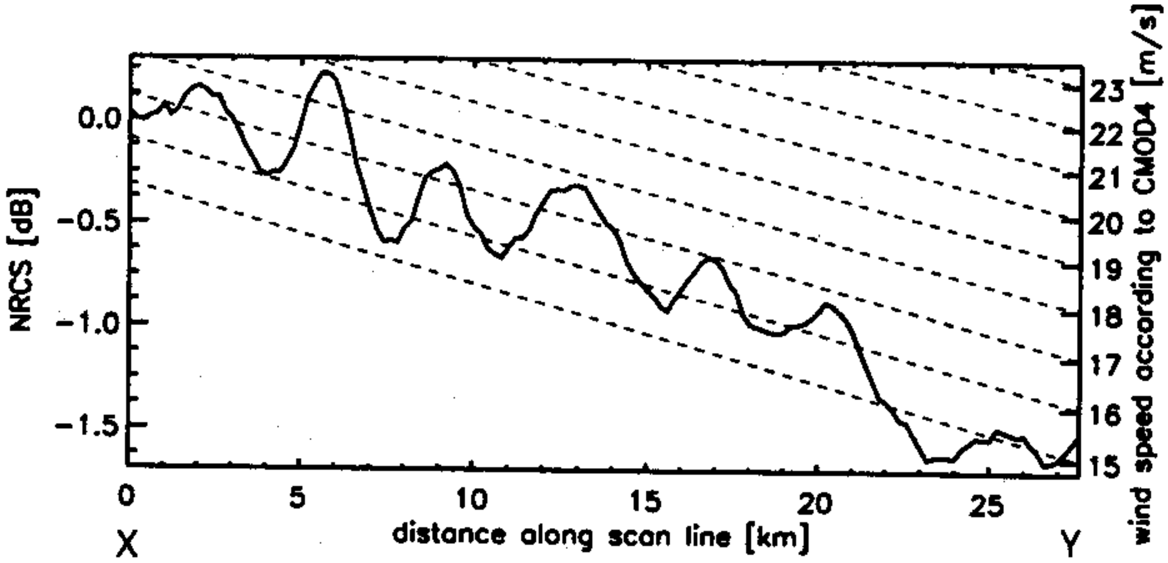

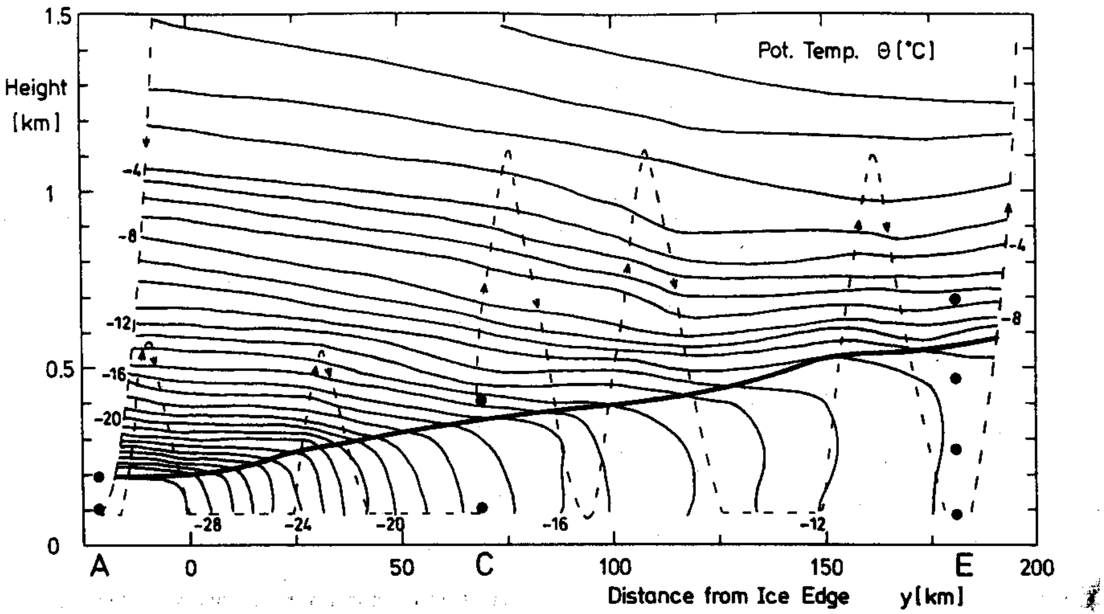

Vertical cross section of potential temperature derived from aircraft measurements.
Thick line is the top of the boundary layer.

Height of the boundary layer is related to the “wavelength” of the wave pattern via the aspect ratio.

Atmospheric eddies

Atmospheric eddy over the Black Sea

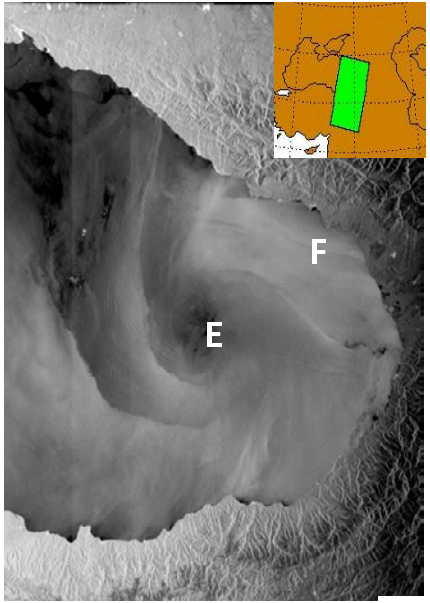

Envisat SAR image 13-08-20210, 0732 UTC over the eastern Black Sea showing radar signatures of a mesoscale atmospheric cyclonic eddy.

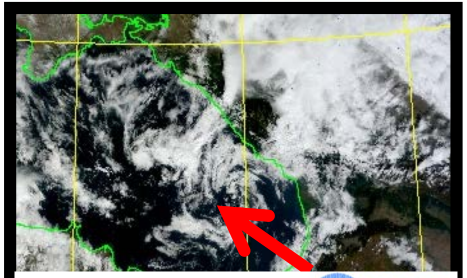

MODIS Terra color composite image, 13-09-2010, 0830 UTC showing in the eastern section of the Black Sea a cyclonic eddy in the cloud pattern (the red arrow points to its center).

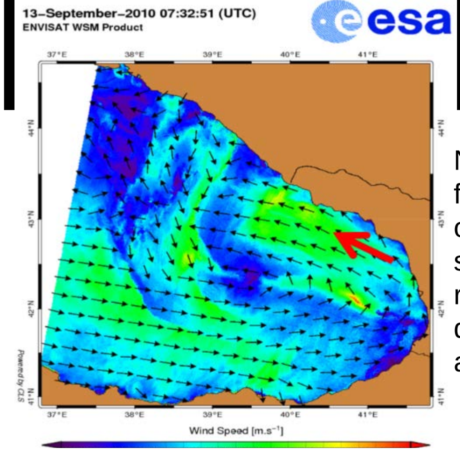

Near-surface wind field derived from the ASAR image depicted on the left by including Doppler shift information in the wind retrieval algorithm. The arrow denotes the wind direction in an area along the east

From Alpers et al., Int. J. Remote Sens., 2015

Land breeze

Land breeze off the west coast of Morocco

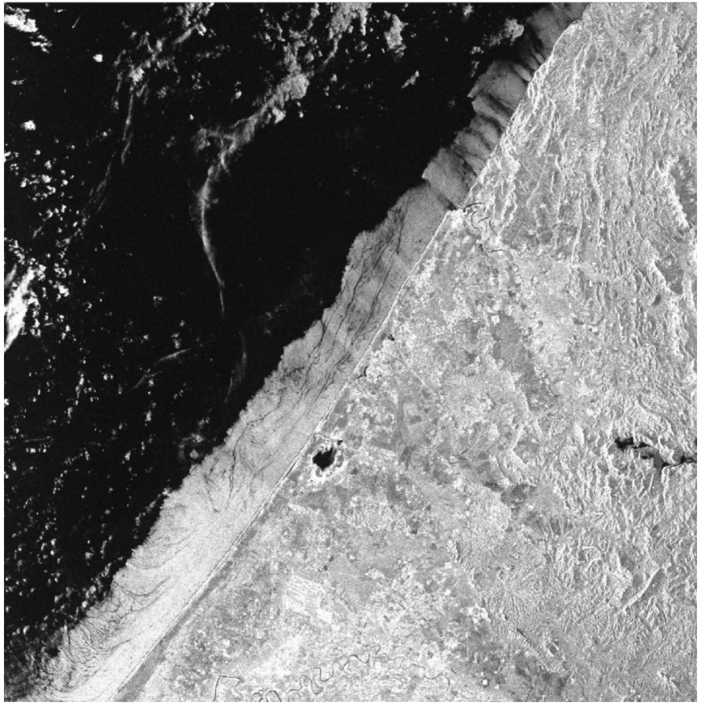

ERS-1 SAR, 06-02-1995, 22:44 UTC

ERS-1 SAR image of the Moroccan Atlantic coast near Larache .The bright band following the coast line is caused by a wind blowing late in the evening and at night from the land onto the sea. This land breeze is caused by the fact that after sunset the air over land cools off faster than over the sea. The air in the northern mountainous area is funnelled through the valleys causing the tongue-like bright patterns on the sea surface.

Katabatic Winds

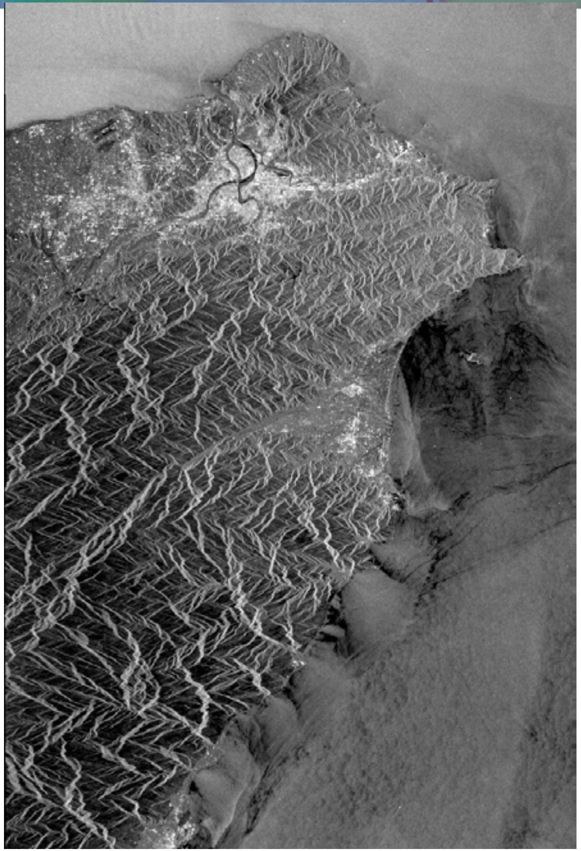

Katabatic Winds off the northeast coast of Taiwan

Envisat ASAR AP image, 10-5-2007,1348 UTC (2148 LST) over the north east coast of Taiwan. The imaged area is 100 km x150 km. Visible are sea surface signatures of katabatic winds attached to the coast.The bright patch in the upper section of the image is Taipei.

Raincells

Rain cell, Gulf of Mexico, Missisippi delta

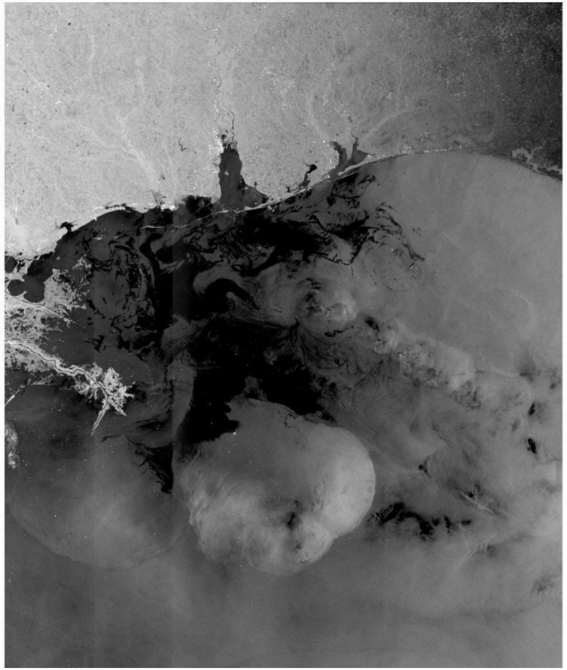

Envisat SAR WS, 2-07-2010, 15:52 UTC

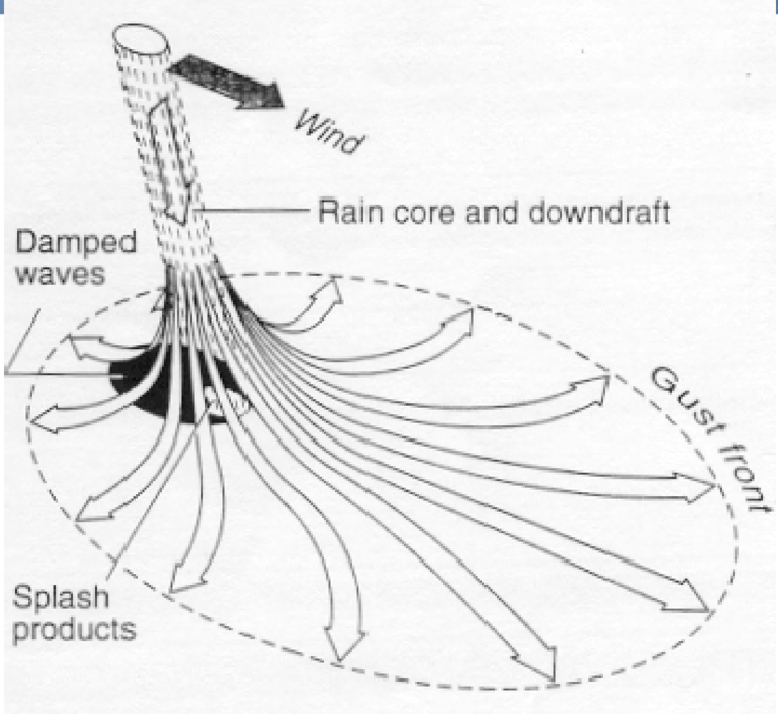
Wind
Rain core and downdraft
Damped waves
Gust front
Splash products

Rain band south of Hong Kong

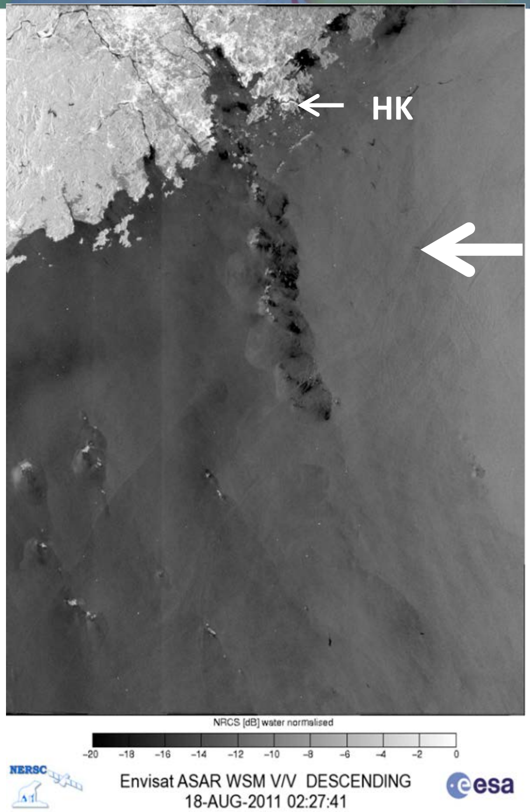

SAR look direction

Envisat SAR images acquired in the Wide Swath Mode (WSM) at VV polarizations during a descending satellite path over the South China Sea south of Hong Kong on 18 August 2011 at 02:27:41 UTC showing the radar signature of a rain band. Inserted is in the image the look direction of the SAR antenna (thick white arrow) and the location of Hong Kong (HK).

Quasi-simultaneous weather radar image

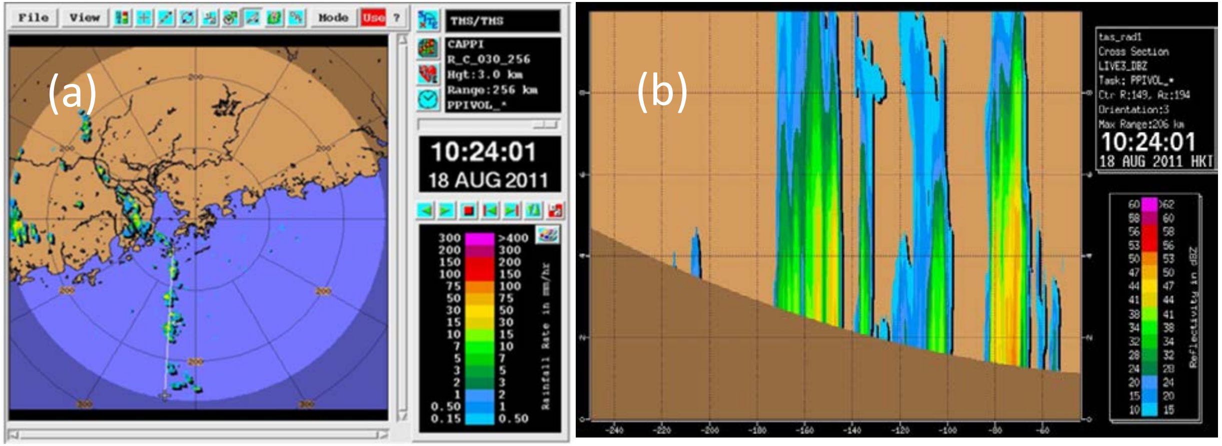

(a) Weather radar image acquired on 18-08- 2011, 02:24 UTC (10:24 LT).
(b) Vertical profile of the radar reflectivity along the transect inserted in the weather radar image.

Stratiform rain off the west coast of Taiwan

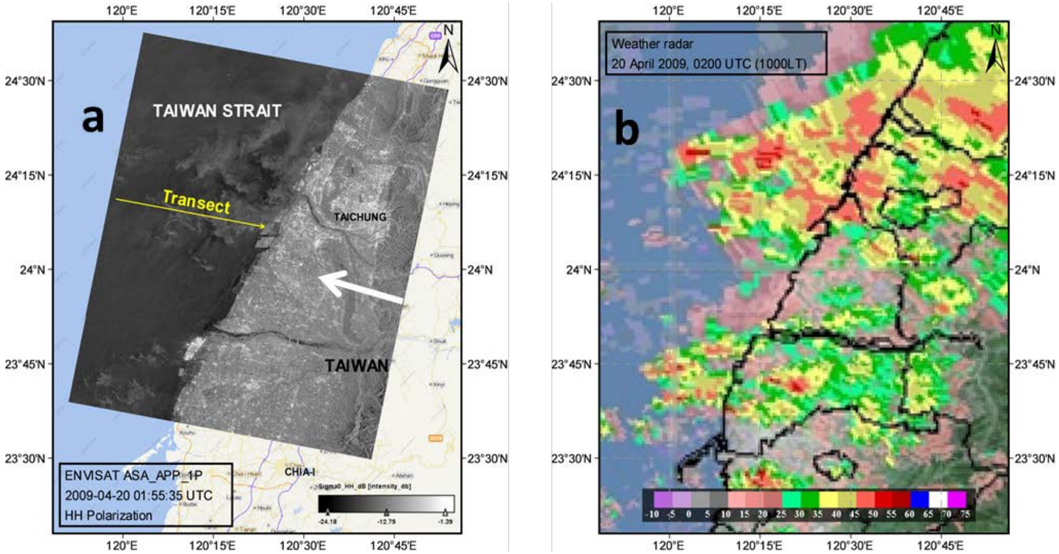

Envisat SAR images acquired in the APP Mode at VV polarizations during a descending satellite path over the Taiwan Strait west of Taiwan on 20-04-2009 ,01:55 UTC, showing the radar signature of a rain. Inserted is the look direction of the SAR antenna (thick arrow) and the transect along which the variation of the NRCS at HH and HV polarizations have been determined, see Fig. 13. (b) Weather radar image acquired on 20-04- 2009, 02:00 UTC (10:00 LT). The rain rate was 12-24 mm h^{-1} (moderate rain) and the ambient wind of 5 m s^{-1} from south.

Stratiform rain off the north coast of Germany

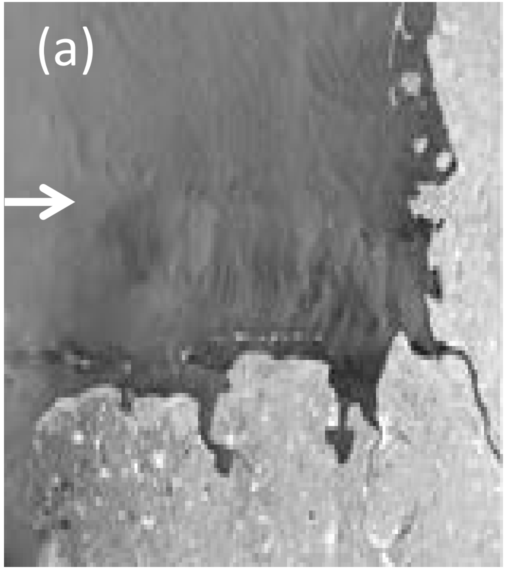

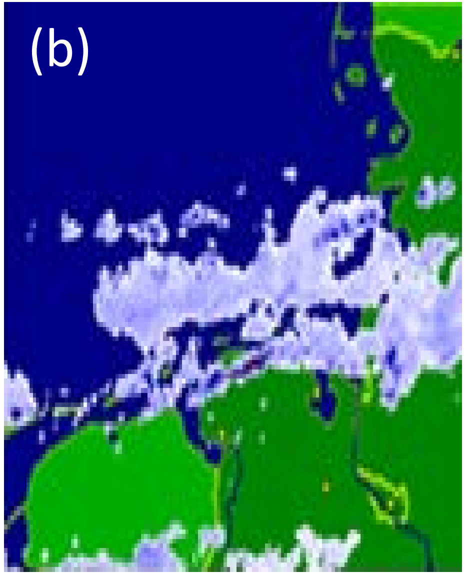

Envisat ASAR image acquired in the Wide Swath Mode (405 m swath width), VV polarization, over the southern North Sea on 09-12-2011, 21:18 UTC, showing the radar signature of a broad rain area. The white arrow denotes the look direction of the SAR antenna. (b) Weather radar image of the German Weather Service acquired on 09-12-2011, 21:15 UTC (22:15 LT). The rain rate was 1-5 mm h^{-1} (light to moderate) and the ambient wind 12- 14 m s^{-1}.

The radar signatures of rain depend strongly on frequency and polarization

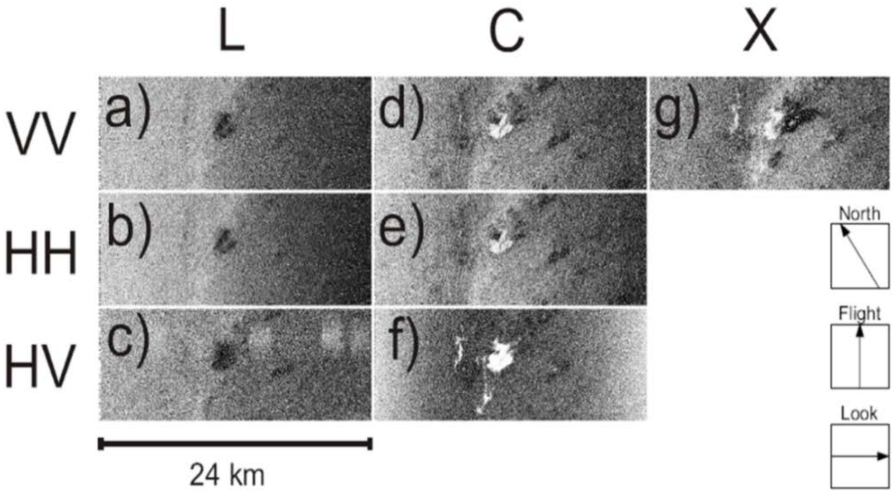

Multi-frequency, multi-polarization SIR-C/X-SAR images acquired simultaneously at L-, C-, and X-band over the Gulf of Mexico on 18 -04-994, 08:11 UTC showing the strong dependence of the radar signature on radar frequency and polarization.

Alpers, Zhang, Mouche, Zheng, Chan; "Rain footprints on C-band synthetic aperture radar images of the ocean – revisited", submitted to Remote Sensing of Environment, Dec. 2015

Conclusions

- Meso-scale atmospheric phenomena in the marine boundary layer become visible on SAR images of the sea surface because they are associated with a variable wind speed at the sea surface.
- Often it is difficult to decide whether features visible on the SAR images result from oceanic or atmospheric phenomena.
- Then additional information is needed, e.g., from other satellites or from the ground.
- SAR images of the sea surface yield detailed information on meso-scale atmospheric phenomena that cannot be obtaind by other means.
- SAR images of the sea surface are of great value for validating meso-scale atmospheric models of the marine boundary layer.

More examples can be found at the website

https://earth.esa.int/web/guest/-/ers-sar-tropical-6036

entitled

“The tropical and subtropical ocean viewed by ERS SAR”

by

Werner Alpers (Hamburg, Germany**)**
Leonid Mitnik) (Vladivostok, Russia)
Lim Hock (Singapore**)**
Kun Kan Chen (Chungli, Taiwan)

Thank you for your attention

谢谢！